



Integration of Remote-Sensing and Geological Data as Aids to Mapping Surficial Sediments in Northwestern Alberta

Integration of Remote-Sensing and Geological Data as Aids to Mapping Surficial Sediments in Northwestern Alberta

S. Mei, M.M. Fenton and R. Paulen

October 2005

©Her Majesty the Queen in Right of Alberta, 2005
ISBN 0-7785-3862-1

The Alberta Energy and Utilities Board/Alberta Geological Survey (EUB/AGS) and its employees and contractors make no warranty, guarantee or representation, express or implied, or assume any legal liability regarding the correctness, accuracy, completeness or reliability of this publication. Any digital data and software supplied with this publication are subject to the licence conditions. The data are supplied on the understanding that they are for the sole use of the licensee, and will not be redistributed in any form, in whole or in part, to third parties. Any references to proprietary software in the documentation, and/or any use of proprietary data formats in this release, do not constitute endorsement by the EUB/AGS of any manufacturer's product.

If this product is an EUB/AGS Special Report, the information is provided as received from the author and has not been edited for conformity to EUB/AGS standards.

When using information from this publication in other publications or presentations, due acknowledgment should be given to the EUB/AGS. The following reference format is recommended:

Mei, S., Fenton, M., Paulen R. (2005): Integration of remote-sensing and geological data as aids to mapping surficial sediments in northwestern Alberta; Alberta Energy and Utilities Board, EUB/AGS Earth Sciences Report 2005-03, 48 p.

Published October 2005 by:

Alberta Energy and Utilities Board
Alberta Geological Survey
4th Floor, Twin Atria Building
4999 – 98th Avenue
Edmonton, Alberta
T6B 2X3
Canada

Tel: (780) 422-3767 (Information Sales)

Fax: (780) 422-1918

E-mail: EUB.AGS-Infosales@gov.ab.ca

Website: <http://www.ags.gov.ab.ca/>

Contents

Contents	iii
Acknowledgments	v
Abstract	vi
1 Introduction	1
2 Study Area	3
2.1 Location and Physiography.....	3
2.2 Bedrock Geology	4
2.3 Glacial History and Stratigraphy	5
3 Methodology	8
4 Image Data and Processing	12
4.1 RADARSAT-1 Images	12
4.2 RADARSAT-1 Images and Principal-Component Images Processed by Resource GIS and Imaging Ltd.	12
4.3 RADARSAT-1 Images Processed in this Study	23
4.4 Digital Elevation Model from Shuttle Radar Topography Mission.....	27
4.5 Landsat Image.....	29
4.6 Indian Remote-Sensing Satellite Image	30
4.7 Data Integration	31
5 Interpretation and Results	33
6 Discussion and Conclusion	39
7 References	41
Appendix A — Ground-Truthing Sites in Map Area NTS 84K	46

Table

Table 1. Covariance eigenvectors of principal-component analysis used by Resource GIS and Imaging Ltd. (RGI).....	18
---	----

Figures

Figure 1. Study area shown on a pseudocolour map of the Shuttle RADAR Topography Mission (SRTM) digital elevation model (DEM). Colour scale represents metres above sea level.	1
Figure 2. Multibeam configuration of RADARSAT-1 S1 and S7 ascending-descending imagery obtained by the Alberta Geological Survey (<i>after</i> Grunsky, 2002a).....	3
Figure 3. Bedrock geology of the study area. Background is a shaded-relief image of the Shuttle RADAR Topography Mission (SRTM) digital elevation model (DEM).....	5
Figure 4. Digital elevation model (DEM) showing streamlined landforms, indicating the latest ice-flow direction. Meltwater channels are also easily seen in this image.	6
Figure 5. Surficial geology of the Mount Watt area (NTS 84K), as mapped by Fox et al. (1987). Background is a Landsat natural-colour image. Legend: 1, eolian sand; 2, alluvial gravel to clay; 3, lacustrine silt and clay; 4, glaciolacustrine silt and clay; 5, glaciofluvial sand to gravel; 6, gravel to clay till; 7, colluvial gravel to clay; 8, organic; 9, bedrock.	7
Figure 6. Alberta Geological Survey classification scheme for surficial geological mapping (<i>from</i> Paulen et al., 2005a).....	9
Figure 7. Alberta Geological Survey genetic and geomorphic modifiers for surficial geological mapping (<i>from</i> Paulen et al., 2005a).	10
Figure 8. RADARSAT-1 Standard Beam 1 ascending pass image (S1A) with an enhanced frost removal transformation using a 9 x 9 kernel.	14
Figure 9. RADARSAT-1 Standard Beam 1 descending pass image (S1D) with an enhanced frost removal transformation using a 9 x 9 kernel.	15

Figure 10. RADARSAT-1 Standard Beam 7 ascending pass image (S7A) with an enhanced frost removal transformation using a 9 x 9 kernel.	16
Figure 11. RADARSAT-1 Standard Beam 7 descending pass image (S7D) with an enhanced frost removal transformation using a 9 x 9 kernel.	17
Figure 12. Principal-component 1 image for 84K processed by Resource GIS and Imaging Ltd. (RGI). .	19
Figure 13. Principal-component 2 image for 84K processed by Resource GIS and Imaging Ltd. (RGI). .	20
Figure 14. Principal-component 3 image for 84K processed by Resource GIS and Imaging Ltd. (RGI). .	21
Figure 15. Principal-component 4 image for 84K processed by Resource GIS and Imaging Ltd. (RGI). .	22
Figure 16. Pseudocolour colour-composite image with the PC3 image as red, PC1 image as green and PC2 image as blue.	23
Figure 17. Image for NTS 84K created by using algorithm $([S1A + S7A] - [S1D + S7D])$	25
Figure 18. Image for NTS 84K created by using algorithm $([S1A + S1D] - [S7A + S7D])$. Displayed in pseudocolour.	26
Figure 19. Image for NTS 84K created by using $([S1A + S7A] - [S1D + S7D])$ image as red, $([S1A + S7A] + [S1D + S7D])$ image as green and $([S1A + S1D] - [S7A + S7D])$ image as blue.	27
Figure 20. Shuttle Radar Topography Mission (SRTM) digital elevation model (DEM) displayed in pseudocolour combined with sunshade relief with a 45° light-direction azimuth and a sun elevation of 45°.	28
Figure 21. Landsat 7 ETM Plus image for NTS 84K.	29
Figure 22. Indian Remote-Sensing Satellite (IRS) panchromatic image for NTS 84K.	30
Figure 23. Image created by integration of the Landsat image, the Indian Remote-Sensing Satellite (IRS) image and Shuttle Radar Topography Mission (SRTM) digital elevation model (DEM).	31
Figure 24. Image created by fusing Shuttle Radar Topography Mission (SRTM) digital elevation model (DEM) with pseudocolour composite image of processed RADARSAT-1 images, using $([S1A + S7A] - [S1D + S7D])$ image as red, $([S1A + S7A] + [S1D + S7D])$ image as green and $([S1A + S1D] - [S7A + S7D])$ image as blue.	32
Figure 25. Image created by fusing Shuttle Radar Topography Mission (SRTM) digital elevation model (DEM) with pseudocolour composite image of processed RADARSAT-1 images, using $([S1A + S7A] - S7D)$ image as red, $([S1A + S7A] - S1D)$ image as green and $([S1A + S7A] / S7D)$ image as blue.	33
Figure 26. Ground-truthing sites shown on the processed RADARSAT-1 image, with $([S1A + S7A] - S7D)$ image as red, $([S1A + S7A] - S1D)$ image as green and $([S1A + S7A] / S7D)$ image as blue.	34
Figure 27. Finger-print-like ridges on a portion of the processed image in Figure 23 around field site MF04-44.	36
Figure 28. Polygonal dimpled pattern on a portion of the processed image in Figure 23 around field site MF04-42.	37
Figure 29. Interpreted surficial geological map superimposed on a shaded-relief image of the Shuttle Radar Topography Mission (SRTM) digital elevation model (DEM). Surficial materials and their boundaries were modified from Fox et al. (1987) by using remote-sensing imagery supplemented with field observations.	38

Acknowledgments

The authors wish to acknowledge the support of the Alberta Department of Sustainable Resource Development for the acquisition of the RADARSAT-1 imagery. Ken Dutchak, Gerry Mitchell and Eric Grunsky provided information on processing the Alberta Geological Survey (AGS) RADARSAT-1 imagery. The authors have benefited from discussions with AGS colleagues John Pawlowicz and Laurence Andriashek during the course of the project. John Pawlowicz and Tami Nicoll are thanked for field assistance. We thank Jeff Harris for technical review and Bob Davie and Gisela Hippolt-Squair for editorial review.

Abstract

The surficial material in northern Alberta is characterized by glacial sediments of the Laurentide Ice Sheet, which are covered by the Northern Boreal Forest. Intensity levels of surficial mapping surveys (field checking methods) in large portions of northern Alberta are constrained by limited road access. Airphoto interpretation, in combination with discontinuous field ground-truthing, becomes the main approach to surficial mapping in the Northern Boreal Forest Plain. To develop a cost-effective mapping approach for such a large inaccessible area, the Alberta Geological Survey (AGS) acquired other remotely sensed data, including RADARSAT-1, Shuttle RADAR Topography Mission (SRTM) digital elevation model (DEM), Landsat and Indian Remote-Sensing Satellite (IRS) images, to support surficial mapping. This study attempts to

- evaluate the applicability of the RADARSAT-1 images to augment ongoing surficial geological mapping programs for northern Alberta; and
- provide a preliminary investigation and interpretation of surficial materials for a selected region of northwestern Alberta by using remote-sensing data, including RADARSAT-1 Standard Beam 1 and 7 images, a DEM from SRTM, a Landsat natural-colour image and an IRS panchromatic image augmented by an existing low-resolution surficial geology map and widely spaced field observations.

The RADARSAT-1 images acquired by AGS are from different incidence angles and look directions. Therefore, moisture and surface roughness information can be extracted by applying algorithms that contrast differences caused by different incidence angles and look directions (ascending versus descending looks). The processed RADARSAT-1 images contain information on surface morphology, moisture and land-cover type, and are therefore useful in surficial geological mapping and complementary to optical satellite images, including Landsat and IRS. The IRS panchromatic image is used to sharpen the Landsat and processed RADARSAT-1 images to obtain a higher resolution. For sunshade relief, the SRTM DEM is fused with the sharpened images to enhance topographic patterns. Then, surficial geology and ice-flow reconstruction are interpreted from the processed images.

Remote-sensing data have proven valuable for fieldwork. The latest satellite images provide the only record of recent development, such as roads, well pads and cut blocks, which is crucial to surficial mapping in areas with little access. The addition of remote-sensing data to the surficial geologist's 'tool box' increases the information available for creating the surficial map. Remote-sensing data, however, do not reduce the resources required, as the most expensive aspect of surficial mapping is the ground-truthing that must be done regardless of the availability of remote-sensing data.

1 Introduction

A study of the application of remote-sensing technology for surficial geological mapping in the Northern Boreal Forest Plain has been undertaken as a contribution to the Alberta Geological Survey (AGS) Quaternary mapping initiative under the Alberta Mineral Strategy (Alberta Energy, 2002) and as a contribution to the Geological Survey of Canada (GSC) Northern Resource Development (NRD) Project 4450. A test site in northwestern Alberta, consisting of the Mount Watt map area (NTS 84K), which contains the community of High Level, was chosen (Figure 1). The High Level region was selected for testing because it represents a typical northern Alberta environment, complete with varying degrees of anthropogenic disturbance (e.g., farming, logging, energy development), a wide variety of surface materials of varied genesis, and surface topography that includes bedrock highlands and broad low-relief valleys containing numerous wetlands. The purpose of this research is to develop new methodologies in support of the production of surficial geology maps using a variety of remotely sensed data. Various types of remote-sensing imagery were analyzed within the test region to evaluate the usefulness of remote-sensing information for assisting surficial geological mapping in remote regions of the Northern Boreal Forest of Alberta.

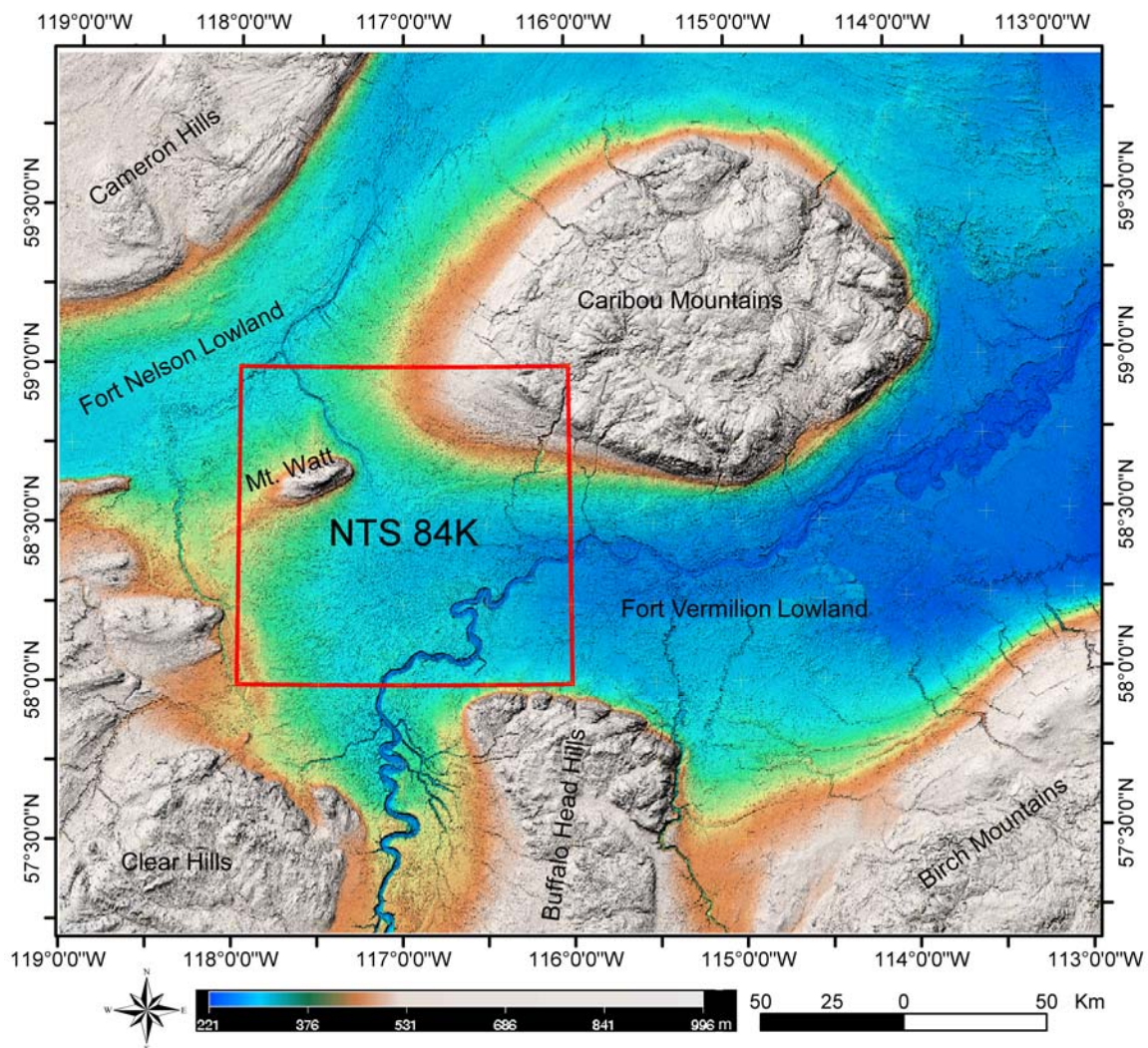


Figure 1. Study area shown on a pseudocolour map of the Shuttle RADAR Topography Mission (SRTM) digital elevation model (DEM). Colour scale represents metres above sea level.

Conventional surficial geological mapping establishes the composition of distinctive landforms based on ground observations. This is aided by interpretation of standard panchromatic airphoto stereopairs, which allows for the sharp delineation landform extent. The airphotos used are available at varying scales and permit differentiation of surficial units typically ranging in area from 0.01 to 1 km² (Sauer and Elder, 1982; Mollard, 1996; British Columbia Resources Inventory Committee, 1996). With mapping experience by the geologist backed by field observations, airphoto interpretation has become the common means of delineating surficial geological map units, sediments and landforms. Extensive vegetation cover in northern Alberta has inhibited the successful use of remote-sensing analysis for surficial mapping in previous studies (Fenton and Weiss, 2003). Although widely used in vegetation-poor regions of Australia and the nonglaciated area of the United States (Sabins, 1992), remote-sensing information, particularly four-beam RADARSAT-1 (ascending and descending Standard Beam 1 and 7) imagery, has not been systematically tested for the purpose of surficial mapping in the heavily vegetated region of the Northern Boreal Forest of western Canada.

Remote-sensing imagery (e.g., Landsat and Synthetic Aperture Radar (ERS-1)) has been commonly employed for mapping geomorphology, geological structure, moisture, terrain and surficial material in areas, including the Canadian Shield, where there is less vegetation cover and/or less overburden (Bélanger, 1980, 1983, 1988; Lowman et al., 1987; Boulton and Clark, 1990; Gupta, 1991; Singhroy et al., 1993; Graham and Grant, 1994; Blais et al., 1995; Kettles et al., 1998; Singhroy and Saint-Jean, 1999; Smith et al., 1999; Harris et al., 2001; Grunsky, 2002a; Eccles et al., 2001; Paganelli and Rivard, 2002; Paganelli et al., 2003; Brown et al., 2005). The AGS acquired RADARSAT-1 images (Grunsky, 2002a, b; Mei, 2004a, b) as part of a strategy to develop a more comprehensive approach to mapping the surficial and structural geology in northern Alberta. The RADARSAT-1 satellite operates at a single microwave frequency of 5.3 GHz (5.6 cm wavelength), generally known as C-band, and the microwave transmission operates in an HH polarization mode (horizontally sending and horizontally receiving) (Luscombe et al., 1993). Unlike images from optical sensors, such as Landsat thematic mapper (TM), Indian Remote-Sensing Satellite (IRS) and *Système Pour l'Observation de la Terre* (SPOT) satellite, which are reflective of chemical and physical properties of imaged objects, backscatter in the RADARSAT-1 imagery is influenced by topography, surface moisture and surface roughness as defined by barren ground, rock and the type of vegetation or forest canopy. These three factors have a complex relationship with one another, complicating the interpretation of backscatter responses. Surface roughness reflects the nature of geomorphology, soil type and underlying glacial sediment. Surficial sediments influence the amount of moisture in the soil, the nature of the soil profile developed and the type of vegetation that is typically associated with the soil. Thus, the backscatter associated with vegetation reflects, in part, the nature of the surficial geology.

The RADARSAT-1 imagery acquired by AGS consists of RADARSAT-1 Standard Beam 1 and 7 in both ascending and descending passes ([Figure 2](#)). As a result, principal component images can be derived from images acquired from these four beam positions (Grunsky, 2002a, b; Mei et al., 2005). Principal-component analysis (PCA) is a classical statistical method that produces images (components) that are a linear combination of the input images (Richards, 1986; Gupta, 1991). Previous studies have shown that principal-component images derived from radar imagery, acquired by the first European Remote Sensing satellite (ERS-1) and the Canada Centre for Remote Sensing (CCRS) C-SAR satellite, with different incidence angles, look directions, frequencies and polarizations, are very useful for highlighting structural features in the Canadian Shield (Masuoka et al., 1988; Moon et al., 1994; Harris et al., 1994, 2001), where the drift cover is relatively thin over the bedrock. Although most studies have focused on the use of radar images for delineating geological structure (Sabins 1992), they have also been used for mapping surficial geology (Graham and Grant, 1994; Barnett et al., 2004). The RADARSAT-1 principal-component imagery of AGS has been used for structural mapping in the central Alberta Foothills (Paganelli and Rivard, 2002), the Buffalo Head Hills area (Eccles et al., 2001; Paganelli et al., 2003) and the Maybelle River area south of Athabasca Lake (Mei et al., 2005), and for land-cover and terrain mapping (Grunsky,

2002b).

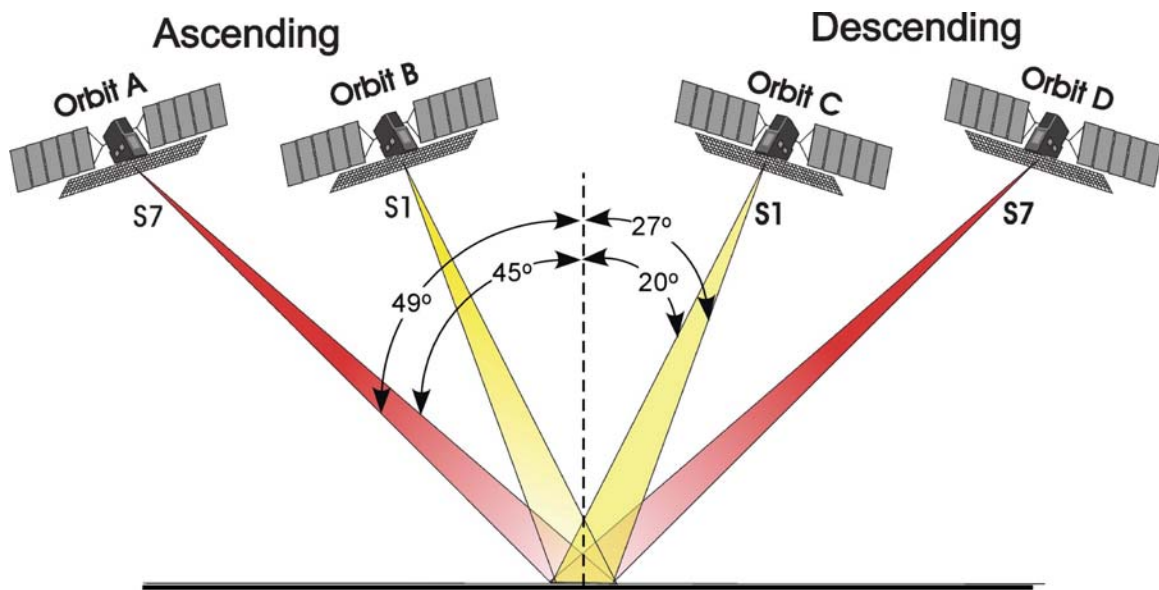


Figure 2. Multibeam configuration of RADARSAT-1 S1 and S7 ascending-descending imagery obtained by the Alberta Geological Survey (after Grunsky, 2002a).

Ultimately, this study has two objectives:

- to evaluate the applicability of interpreting the RADARSAT-1 images for surficial geological mapping in northern Alberta
- to provide preliminary surficial geological information for regional surficial geological mapping in northwestern Alberta using remotely sensed data, including RADARSAT-1 Standard Beam 1 and 7 images, the digital elevation model (DEM) from the Shuttle RADAR Topography Mission (SRTM), Landsat natural-colour images and IRS panchromatic images.

The approach adopted consists of 1) image processing and fusion of available RADARSAT-1 images, DEM from SRTM, Landsat and IRS images to extract geomorphological, moisture, glacial and land-cover information; 2) interpretation of the processed images and delineation of surficial-material boundaries by experienced surficial geologists; and 3) some ground validation by field observations.

2 Study Area

2.1 Location and Physiography

Located in northwestern Alberta, the Mount Watt map area (NTS 84K; [Figure 1](#)) extends from latitude 58° to 59°N and from longitude 118° to 116°W, and occupies portions of the Northern Alberta Lowlands and Uplands regions (Bostock, 1970) of the Canadian Interior Plains. These regions are subdivided in the Mount Watt map area into two main lowland regions: the Fort Vermillion Lowland in the central and eastern portions of the map area and the Fort Nelson Lowland to the northwest (Pettapiece, 1986). The lowland regions are bounded by the Clear Hills Uplands to the southwest, the Cameron Hills Uplands to the northwest, the Caribou Mountains to the northeast and the Buffalo Head Hills to the southeast (Pettapiece, 1986). Mount Watt occurs as an isolated upland northeast of the Clear Hills Uplands. Elevations range from 350 m above sea level (asl) in the Peace River Valley to about 945 m asl in the

Caribou Mountains to the northeast. All streams southeast of Mount Watt drain into the Peace River, which is characterized by a confined meandering fluvial valley to the southwest and a broad meandering braided plain to the northeast. The Peace River flows northeastward and joins the Slave River north of Lake Athabasca. North of Watt Mountain, all streams flow into the Hay River system, a confined river valley flowing northward to Great Slave Lake.

The lowland plains are characterized by low undulating relief and the surficial materials are dominated by fine-grained glaciolacustrine sediments. As a result, extensive wetland environments have developed due to poor internal drainage conditions. There is little fluvial dissection of the landscape, which is instead characterized by expansive fen and bog deposits. The Caribou Mountains Upland is dominated by permafrost-rich wetlands and numerous lake-filled depressions.

The study area, excluding areas of agricultural development, is blanketed by Boreal forest and extensive bogs and fens. Forest stands, of varying proportions of trembling aspen, balsam poplar, white birch, white spruce and balsam fir, occupy relatively well-drained uplands. Black spruce in association with tamarack dominates in fens and bogs. Jack pine occupies the sandy terrain in the southeastern part of the study area. Soils are generally poorly drained, commonly with shallow water tables, reflecting the high clay content of the tills (10%–40%) and glaciolacustrine sediment on which they have formed. Grey Luvisols predominate in raised areas, where soil development is more advanced. Static and Turbic Cryosols are found in regions of sporadic discontinuous permafrost, and Solonetzic soils are found in areas of thin drift overlying marine shale bedrock (Lindsay et al., 1960).

2.2 Bedrock Geology

The bedrock of the study area is characterized by a Cretaceous succession composed, in ascending order, dominantly of marine silty shale of the Loon River Formation, marine shale of the Shaftesbury Formation, deltaic to marine sandstone of the Dunvegan Formation and marine shale of the Smoky Group (Green et al., 1970; Hamilton et al., 1999). Shaftesbury Formation shale and siltstone occupy the southwestern and northeastern parts of the study area ([Figure 3](#)). Sandstone of the Late Cretaceous Dunvegan Formation overlies Shaftesbury shale and is exposed on the top of Mount Watt and on the flanks of the Caribou Mountains. Shale of the Late Cretaceous Smoky Group is exposed on the top of the Caribou Mountains. Late Paleogene (Tertiary) quartzite gravel has been reported on top of the Caribou Mountains (Bayrock, 1961; Edwards and Scafe, 1996) and also occurs to the northeast in the Whitesands (NTS 84O) map area.

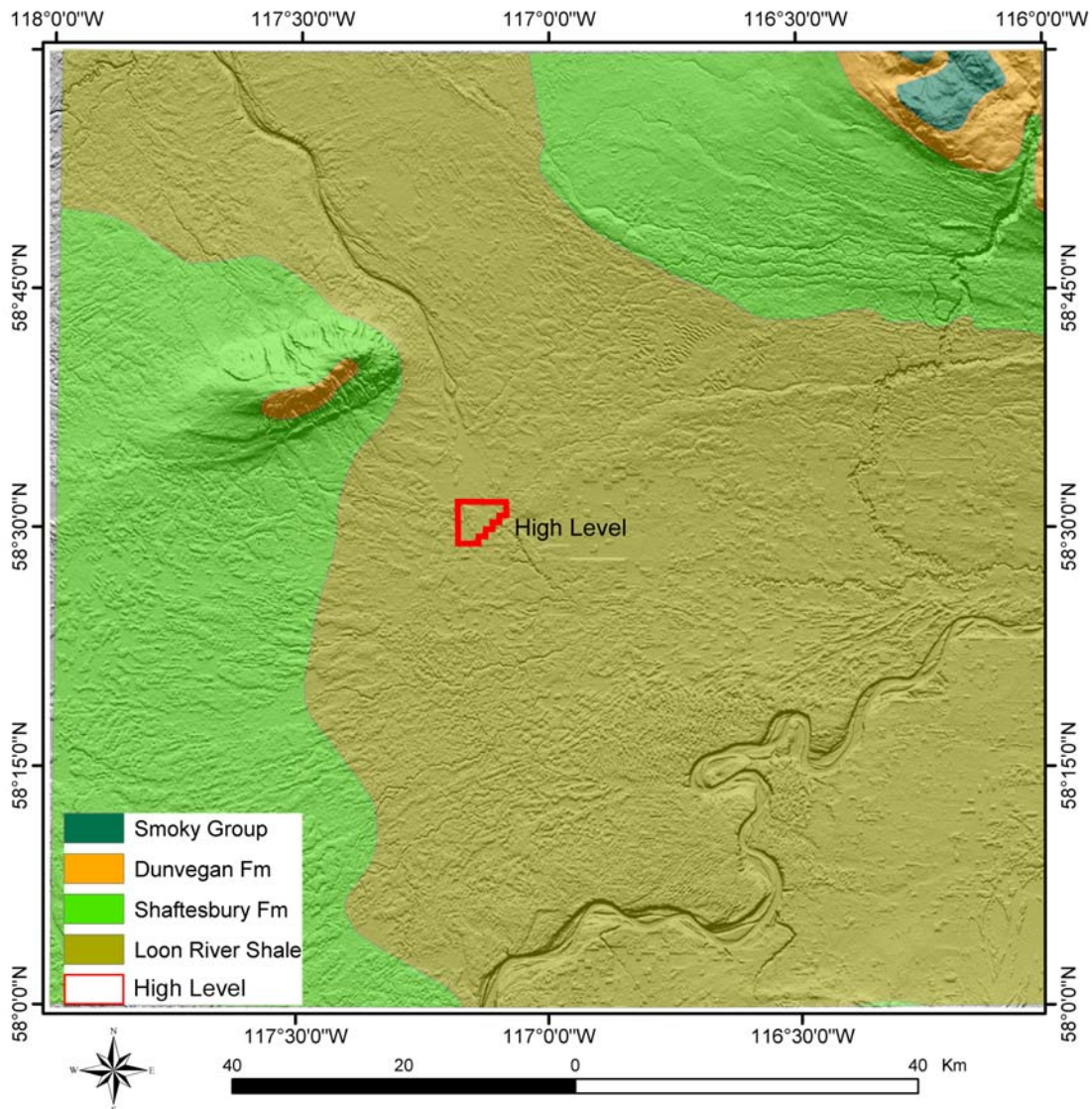


Figure 3. Bedrock geology of the study area. Background is a shaded-relief image of the Shuttle RADAR Topography Mission (SRTM) digital elevation model (DEM).

2.3 Glacial History and Stratigraphy

The present-day landscape of northwestern Alberta is the result of a minimum of two glacial cycles (Fenton et al., 2003a), whereby ice from the Laurentide Ice Sheet advanced from the northeast, filling preglacial drainage systems with glacial sediment. Only glacial sediments from the last glacial event, the Lostwood glaciation (Fenton, 1984), are exposed in the study area. A reconnaissance surficial geology map including the Watt Mountain map area was produced by Fox et al. (1987). Recently, more detailed surficial mapping for the area immediately to the west (Zama Lake, NTS 84L) was completed (Plouffe et al., 2004; Paulen et al., 2005a, b; Smith et al., 2005).

The onset of the Lostwood glaciation in northern Alberta began with the Laurentide Ice Sheet advancing from the northeast (Figure 4). Chronological constraint on the advance of ice is provided by a radiocarbon date of $24\,400 \pm 150$ yr. BP (sample Beta 183598) on wood recovered from gravel underlying late

Wisconsinan till in the adjacent region of northeastern British Columbia (Levson and Ferbey, 2004; Levson et al., 2004) and a $22\,020 \pm 450$ yr. BP (sample AECV-719C) date from a mammoth tusk recovered from the High Level area (Bobrowsky and Rutter, 1992; Burns, 1996). At glacial maximum, regional ice flow was to the west-southwest, with deviations up to 45° (Fenton et al., 2003b). Retreat of ice from the area largely occurred between 11 500 and 11 000 yr. BP (Lemmen et al., 1994; Dyke, 2004).

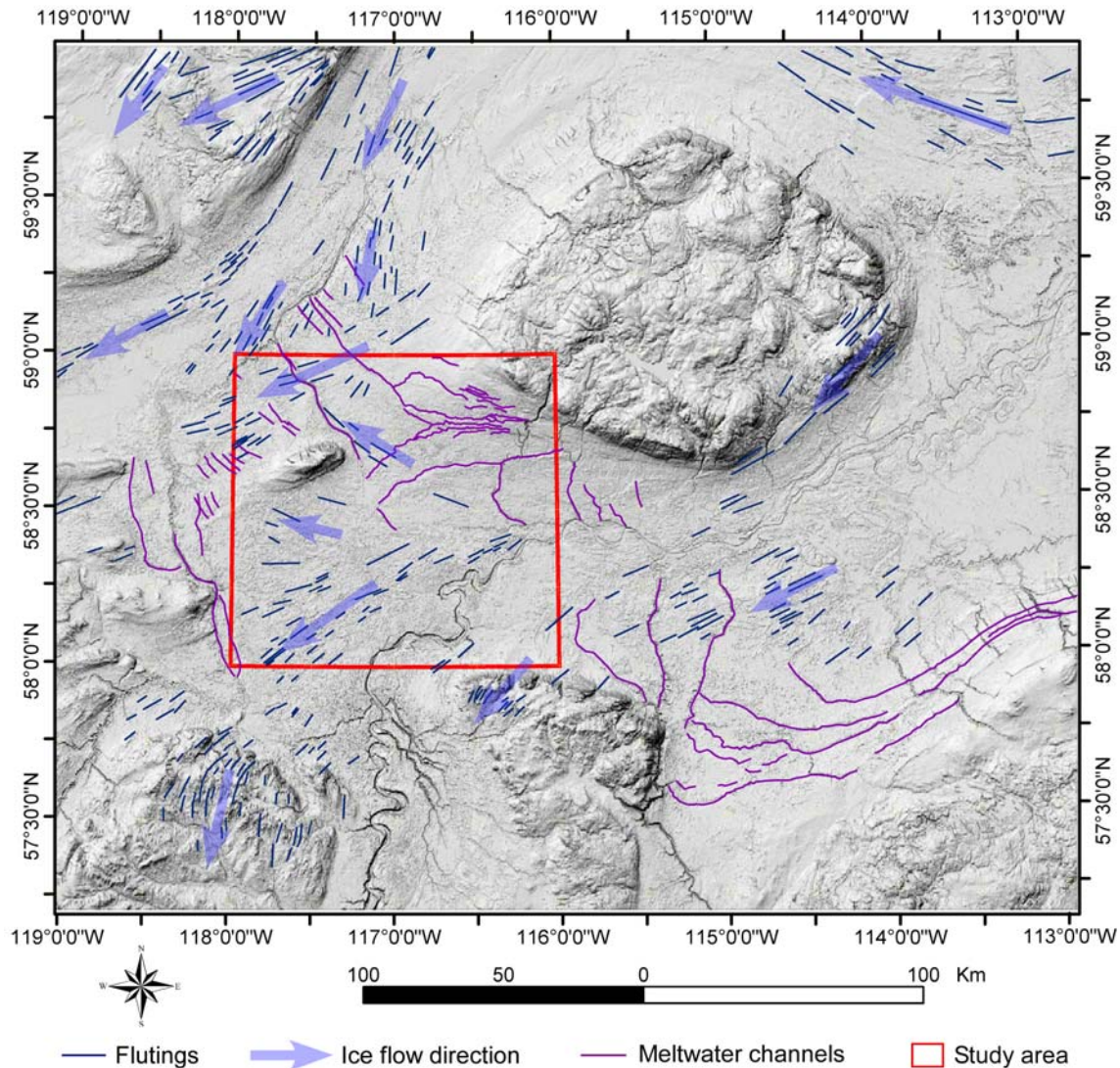


Figure 4. Digital elevation model (DEM) showing streamlined landforms, indicating the latest ice-flow direction. Meltwater channels are also easily seen in this image.

As discussed by Smith et al. (in press), the eastward drainage of regional rivers would have been impounded during the ice advance phase, leading to development of large proglacial lakes. These were progressively displaced by ice, which then deposited a blanket of distinctly clay-rich till across much of the region. The high clay content of this till reflects glacial erosion and entrainment of regional shale-rich bedrock and reworking of advance-phase glaciolacustrine sediment. Characteristics of this diamicton suggest that it is most likely a lodgment depositional environment (cf. Dreimanis, 1988). A second thinner and distinctly sandier till overlies this basal clay-rich till. Fabrics in the two tills tend to be very similar and contacts between them are often diffuse, suggesting that the second till is a facies related to deposition of a greater component of distal (Canadian Shield-derived) coarser englacial sediment, rather

than to a different direction of ice movement. This upper diamicton is interpreted as an ablation till deposit, resulting from deposition by stagnating glacial ice (cf. Dreimanis, 1988).

During deglaciation, large proglacial lakes formed in lowland basins along the retreating ice margin (Mathews, 1980; Lemmen et al., 1994; Dyke, 2004). Extensive blankets of fine-grained glaciolacustrine sediment were deposited in the Hay River and Peace River basins, in glacial lakes Hay and Peace, respectively (Figure 5). Outlets of glacial lake drainage are inscribed upon the landscape, most notably the large drainage channels of glacial Lake Peace, which extend from north of High Level past the eastern side of Watt Mountain and have captured the Hay River drainage to the north (Figures 4, 5). The Meander River spillway (which joins the Hay River) marks the final northward drainage of glacial Lake Peace in the region (Mathews, 1980).

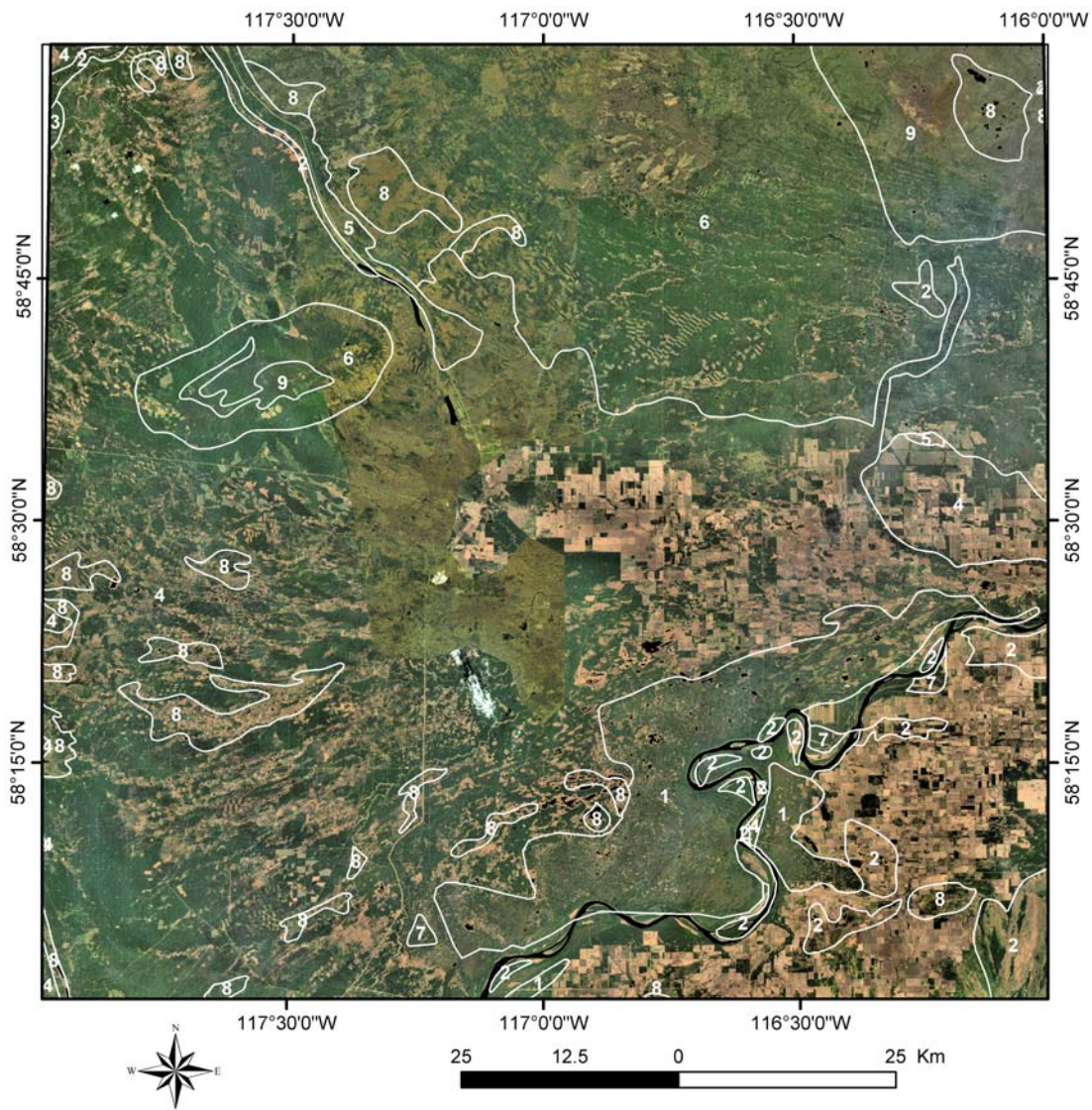


Figure 5. Surficial geology of the Mount Watt area (NTS 84K), as mapped by Fox et al. (1987). Background is a Landsat natural-colour image. Legend: 1, eolian sand; 2, alluvial gravel to clay; 3, lacustrine silt and clay; 4, glaciolacustrine silt and clay; 5, glaciofluvial sand to gravel; 6, gravel to clay till; 7, colluvial gravel to clay; 8, organic; 9, bedrock.

Following the drainage of glacial Lake Peace, early Holocene off-ice winds reworked the sandy littoral glaciolacustrine deposits into a large dune field south of High Level ([Figure 5](#)). These dunes are now stable but thought to have been reworked several times in the Holocene due to drought (Wolfe, 2002). Older dune orientations correspond to southwest and northwest wind directions, with the most recent stabilized dune orientation corresponding to westerly wind directions.

Peatlands and boreal forest occur throughout the study area. Extensive permafrost (i.e., ground that has been frozen year round for more than two years) is considered to have existed following deglaciation, as evidenced by widespread polygonal patterning in fine-grained glaciolacustrine sediment and peatlands. Although much of this is considered relict, discontinuous permafrost is present in the region today, as indicated by active thermokarst, which is distinguished by irregular ground surfaces due to the melting of ground ice. Peatland initiation for northwest Alberta is thought to have occurred immediately after deglaciation, sometime prior to 8 000 yr. BP (Halsey et al., 1998).

3 Methodology

The AGS has developed a classification scheme for surficial geological mapping in northern Alberta (e.g., Paulen et al., 2005a). The descriptions of the various types of surficial materials are included as [Figure 6](#) for convenience of discussion. In addition to the types of surficial material, genetic and geomorphic modifiers are also utilized ([Figure 7](#)).

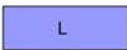
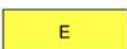
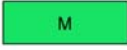
UNIT	UNIT NAME	DESCRIPTION AND GENESIS
QUATERNARY HOLOCENE		
	A	ANTHROPOGENIC MATERIALS: Culturally-made or modified geological materials such that their physical properties (e.g., structure, cohesion, compaction) have been drastically altered.
	O	ORGANIC DEPOSITS: Undifferentiated peat layers, woody to fibrous muck; occurring in undifferentiated wetlands; commonly underlain by fine-grained, poorly-drained glaciolacustrine deposits; includes marshes, swamps, bogs and fens.
	OB	Bog peat: Occurs in a peatland with a fluctuating water table and commonly a raised surface; peatland surface is dominated by sphagnum mosses, heath shrubs and short, stunted trees.
	OF	Fen peat: Occurs in a peatland with water table at surface and slow internal drainage; peatland surface is dominated by sedges, with grasses and reeds near local pools, and sparsely treed.
	C	COLLUVIAL DEPOSITS: Materials that have reached their present position as a result of direct, gravity-induced movement; commonly occurs as slope and slump deposits confined to valley slopes and floors; includes pre-existing bedrock, till, glaciolacustrine, glaciofluvial and eolian sediments, generally poorly sorted.
	F	FLUVIAL DEPOSITS: Sediments transported and deposited by streams and rivers; synonymous with alluvial. Includes well-sorted stratified sand, gravel, silt, clay and organic sediments occurring in channel and overbank deposits (e.g., postglacial floodplains, terraces, fans and deltas).
	L	LACUSTRINE DEPOSITS: Sediments deposited in and adjacent to recent lakes; offshore sand, silt and clay, minor organic deposits; littoral (nearshore beaches and bars) sand and silt and minor gravel.
	E	EOLIAN DEPOSITS: Wind-deposited sediments; well-sorted, medium- to fine-grained sand, and minor silt (loess); generally massive to locally cross-bedded or ripple laminated; includes both active and vegetated deposits.
PLEISTOCENE		
	LG	GLACIOLACUSTRINE DEPOSITS: Fine-grained distal sediments deposited in or along the margins of glacial lakes, including sediments that were released by the melting of floating ice. Includes laminated (rhythmically bedded) to massive fine sand, silt and clay, and may contain ice-rafted stones.
	LGL	Littoral and nearshore sediments: Massive to stratified well-sorted silty sand, pebbly sand and minor gravel; occurs as beaches, bars, spits and foreset deltaic deposits deposited during regression and lowering of glacial lakes.
	FG	GLACIOFLUVIAL DEPOSITS: Sediments deposited by glacial meltwater streams directly in front of glacier ice as subaerial or subaqueous outwash. Includes sand and gravel, often stratified, minor silt, and may show evidence of ice melting (slumped structures). Features include meltwater channels, kettle holes and terraces.
	FGI	Ice-contact sediments: Sediments deposited by glacial meltwater streams in direct contact with glacial ice, either in front of (kame terraces) or within glacial ice (eskers, crevasse ridges). Includes massive to stratified, poor to moderately sorted coarse sediments (predominantly pebble gravel and coarse sand, locally till) and may show evidence of ice melting (slumped structures).
	M	MORAINE: Material deposited directly by glacial ice without modification by any other agent of transportation. Includes nonsorted diamicton deposited as lodgement till (a mixture of clay, silt, sand and minor pebbles, cobbles and boulders) at the ice margin or beneath a glacier. Locally, it may contain blocks of bedrock, pre-existing stratified drift and till. Beds and lenses of glaciolacustrine and/or glaciofluvial sediments may occur.
	MS	Stagnant ice moraine: Terrain resulting from the collapse and lateral movement of englacial and supraglacial sediment in response to melting of buried stagnant ice at the ice margin; sediment is mainly diamicton (till), but locally includes stratified sediments of glaciolacustrine or glaciofluvial origin. Characterized by low- to high-relief hummocky topography.
	MT	Ice-thrust moraine: Terrain resulting from glacio-tectonic transport of originally subglacial sediment and deposited by the glacier more or less intact; deposits may include syngenetic till as well as masses of deposited pre-existing till, stratified drift and/or bedrock. Characterized by high to moderate relief and features include hill-hole pairs and glacio-tectonic moraine ridges.
	MF	Fluted moraine: Glacially streamlined terrain; varies from alternating furrows and ridges to nearly equidimensional smoothed hills; all landforms parallel to the local ice flow direction; includes flutes, drumlins and drumlinoids.
	FP	PREGLACIAL FLUVIAL DEPOSITS: Sediments transported and deposited by streams and rivers prior to glaciation. Includes sand and gravel deposits occurring in paleovalleys (i.e. preglacial floodplains, terraces, fans and deltas); ranging in age from Middle Wisconsin to Late Tertiary.
PRE-QUATERNARY		
	R	BEDROCK: Undivided; may include crystalline (Shield), carbonate or clastic sedimentary rock, and/or coal.
	RT	Fluvial gravels: Predominately well-sorted, quartzite and chert gravel and cobbles; Cordilleran source, Tertiary age.

Figure 6. Alberta Geological Survey classification scheme for surficial geological mapping (from Paulen et al., 2005a).

2005). Unfortunately, the study area is lacking in some of the characteristic glacial landforms. This poses some limitations on the test of applicability of the remote-sensing approach. The surficial materials are also associated with variable moisture contents, which result in characteristic vegetation type and density. For example, glaciolacustrine clay in the lowland tends to be covered by black spruce peat bogs, whereas sand dune fields tend to be covered by jack pine forest stands with very thin organic soil cover.

As mentioned previously, the RADARSAT-1 images acquired by the AGS are from different incidence angles and look directions. As a result, surface topographic information, which is possibly useful for identification of surficial material and landforms, can be extracted by applying algorithms that contrast differences caused by look directions (Mei et al., 2005). Since the slope facing the radar tends to result in high radar backscatter and the slope facing away from the sensor tends to result in low radar backscatter, the contrast between the look directions contributes to an enhanced sunshade relief effect. Principal component analysis has been previously applied to AGS RADARSAT-1 images (Grunsky, 2002b; Paganelli et al., 2003; Mei et al., 2005). The first principal component (PC1) image contains positive contributions from all the input images (Grunsky, 2002b; Paganelli et al., 2003). It highlights differences in land cover type (Grunsky, 2002b). Paganelli et al. (2001, 2003) indicated that the second principal component (PC2) image enhances topographic patterns and surface texture. Grunsky (2002b) concluded that topographic features are best highlighted in the third principal component (PC3) image, and that the discrimination of topographic features using the PC3 image is superior to any other optical commercial satellite imagery with similar spatial resolution. This discrepancy can be explained by the fact that correlation eigenvectors used for principal component analysis change with study areas. In the study of Grunsky (2002b), it was the PC3 image that represented best the contrast caused by look directions. In the study of Paganelli et al. (2003), it was the PC2 image that represented best the contrast caused by look directions. Mei et al. (2005) demonstrated that surficial topographic information can be extracted from RADARSAT-1 Standard Beam 1 and 7 images in both ascending and descending passes by directly applying simple algorithms to contrast the difference between images from the different looking directions, and that the PC2 and PC3 images are not necessarily superior to the images derived directly from the simple algebraic algorithms. Mei et al. (2005) also pointed out that the fourth principal component (PC4) image is characterized by the contrast between the look directions of one beam position (S1 or S7) that is offset by the contrast between the look directions of the other beam position. Consequently, the PC4 image contains much less topographic information than the PC2 and PC3 images.

As opposed to the SRTM DEM, which reflects regional and local topography, the processed RADARSAT-1 images of contrast from the opposite looking directions highlight mainly the surface relief in terms of surface roughness (Mei et al., 2005). In the present study, a DEM from the Shuttle Radar Topography Mission (SRTM) was acquired for highlighting the topography of the study area. Processed RADARSAT-1 images and the SRTM DEM were combined to produce images with both topography and surface relief information (*see below*).

In addition to surficial relief information, wetland information can also be extracted from the RADARSAT-1 images by applying algorithms that contrast differences caused by different incidence angles. Due to high moisture content, radar signal has minimum penetration and is mostly reflected away from the wetlands. Since wetlands tend to be flat and low-relief topography compared to the surrounding areas, the radar backscatter is very sensitive to incidence angles. A shallow incidence angle generally results in more radar signal reflecting away from the sensor, and a steep incidence angle usually results in a higher backscatter to the sensor. There are numerous types of wetlands with different structures in the study area, and a detailed study of the interaction among radar backscatter, incidence angle and wetland structure is beyond the scope of the present study due to time limitations. Nevertheless, it can be established that wetlands generally have a low grey value in RADARSAT-1 Standard Beam 7 (S7) images, which are generated from an incidence angle ranging from 45° to 49°, and have a much higher grey value in RADARSAT-1 Standard Beam 1 (S1) images, which are generated using an incidence angle

ranging from 20° to 27° (Figure 2). In contrast to the wetland, radar backscatter from poplar forest stands tends to be less sensitive to the incidence angles, due to volume scatter of the canopy. This results in a similar grey value of forest stands in both the S1 and S7 images. Consequently, the contrast between S1 and S7 images can be used for differentiating wetlands from forested terrains. Grasslands, cut lands, roads and burns are relatively flat and therefore act in a similar way to the wetland, resulting in similar tones in RADARSAT-1 images. They can also be discriminated from forested lands.

In addition to RADARSAT-1 images and the SRTM DEM, a natural-colour Landsat 7 Enhanced Thematic Mapper (ETM) Plus image and an Indian Remote-Sensing Satellite (IRS) panchromatic image were also used for extracting information on land cover type. The Landsat image provides a natural summer view of the study area, and the IRS image is used to sharpen the Landsat image to obtain an effective resolution of 5.8 m. A major contribution of remote-sensing data to the surficial mapping program is the provision of up-to-date 'road and development' maps of the various regions. The most recent natural-colour Landsat 7 Enhanced Thematic Mapper (ETM) Plus image provides detailed information on recent development, such as roads, well pads and cut blocks. This type of information is important for effective and efficient mapping of areas with limited access. The methodology developed in the present study consists of 1) image processing to extract geomorphic features and wetland information from multibeam RADARSAT-1 images and an SRTM DEM; 2) fusion of processed RADARSAT-1 images, Landsat and IRS panchromatic images with the SRTM DEM to obtain enhanced topography, a natural summer view and higher effective spatial resolution; 3) interpretation of the processed images and delineation of surficial material boundaries by experienced surficial geologists; and 4) ground validation by field observations.

4 Image Data and Processing

4.1 RADARSAT-1 Images

This study uses the RADARSAT-1 images to extract surface geomorphic features and wetland and forest information for interpretation of surficial geology. The processes include applying principal-component analysis and different algorithms to the RADARSAT-1 images. The RADARSAT-1 images over northern Alberta (north of latitude 55°N) comprise two incidence angles, Standard Beam 1 (S1; 20–27°) and Standard Beam 7 (S7; 45–49°), and two look directions, east for ascending pass and west for descending pass (Figure 2). RADARSAT International (RSI) refers to this type of imagery as Synthetic Aperture Radar Georeferenced Fine resolution (SGF) images (RADARSAT International, 1999). The imagery is provided at a nominal resolution of 12.5 m (pixel size), although the true spatial resolution of the Standard Beam image is closer to 25 m. The SGF imagery is calibrated, but remains oriented in the direction of the orbit path. It is sampled in unsigned, 16-bit integer format and written in Committee of Earth Observation Satellites (CEOS) standard format. The strategy of acquiring S1 and S7 imagery was carried out to contrast the radar responses based on two incidence angles and two look directions. The images were obtained in a dry autumn (September to December 1999) and thus provided ideal conditions of no to little deciduous foliage or snow.

4.2 RADARSAT-1 Images and Principal-Component Images Processed by Resource GIS and Imaging Ltd.

The acquired SGF scene images were individually orthorectified by Resource GIS and Imaging Ltd. (RGI; now known as PhotoSat) and then tiled into twenty-five 1:250 000 scale NTS map areas that cover all of northern Alberta north of latitude 55°N. This results in four RADARSAT-1 images, one from each of the beam positions, for each NTS map area (i.e., Standard Beam 1 ascending image (S1A), Standard Beam 1 descending image (S1D), Standard Beam 7 ascending image (S7A) and Standard Beam 7

descending image (S7D)). As well, the four RADARSAT-1 images for northern Alberta were further processed by PhotoSat using principal-component analysis (PCA) with a covariance matrix. As a result, the first four principal-component images were generated for each NTS map area.

The orthorectification was performed using digital elevation data provided by the Resource Data Division (RDD) of the Alberta Department of Sustainable Resource Development. The digital elevation data used have a 100 m grid. Ground control points (GCPs) were collected from 1:20 000 Alberta Access Vectors and an Alberta mosaic of orthorectified Indian Remote-Sensing Satellite (IRS) images, which were also provided by RDD. An average root-mean-square error of 20 m was obtained for the orthorectification. The orthorectified images were then compiled into mosaics. For the S1 mosaics, the near-nadir sides of the images were favoured in the mosaic process; for the S7 mosaics, the off-nadir sides of the images were favoured. This maximizes the incidence angle difference between the S1 and S7 mosaics. Radiometric differences between adjacent images were minimized using two-dimensional, piecewise linear gain and offset adjustment functions, which were interactively adjusted to achieve an optimum balance.

The four RADARSAT-1 Standard Beam 1 and 7 mosaic images for NTS 84K are shown in [Figures 8 to 11](#). A filter (Enhanced Frost Speckle Filter in Geomatica software from PCI Geomatics) was applied to remove high-frequency noise (speckle) while preserving high-frequency features (edges). A kernel of 9 pixels by 9 pixels was used for the filter.

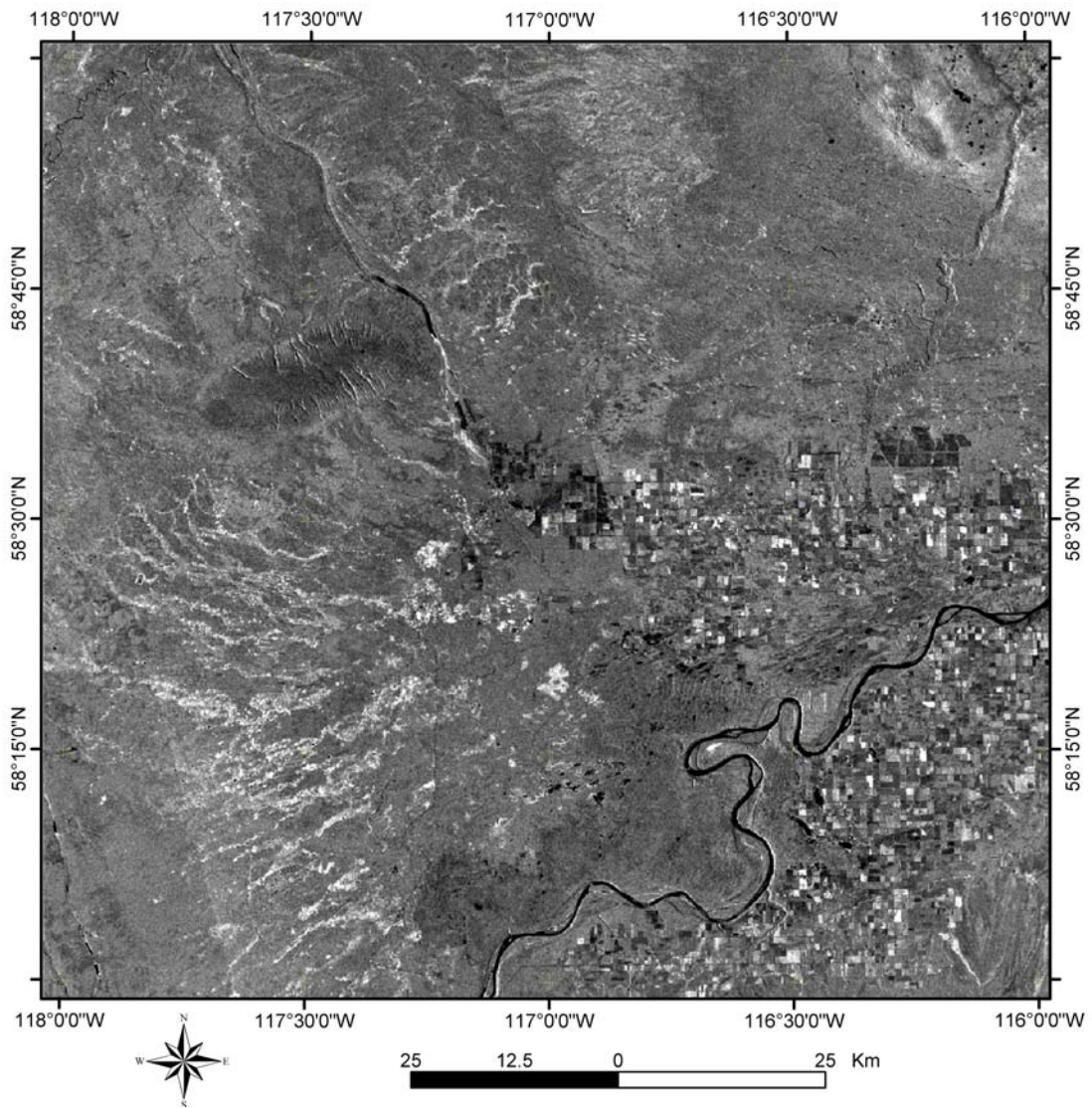


Figure 8. RADARSAT-1 Standard Beam 1 ascending pass image (S1A) with an enhanced frost removal transformation using a 9 x 9 kernel.

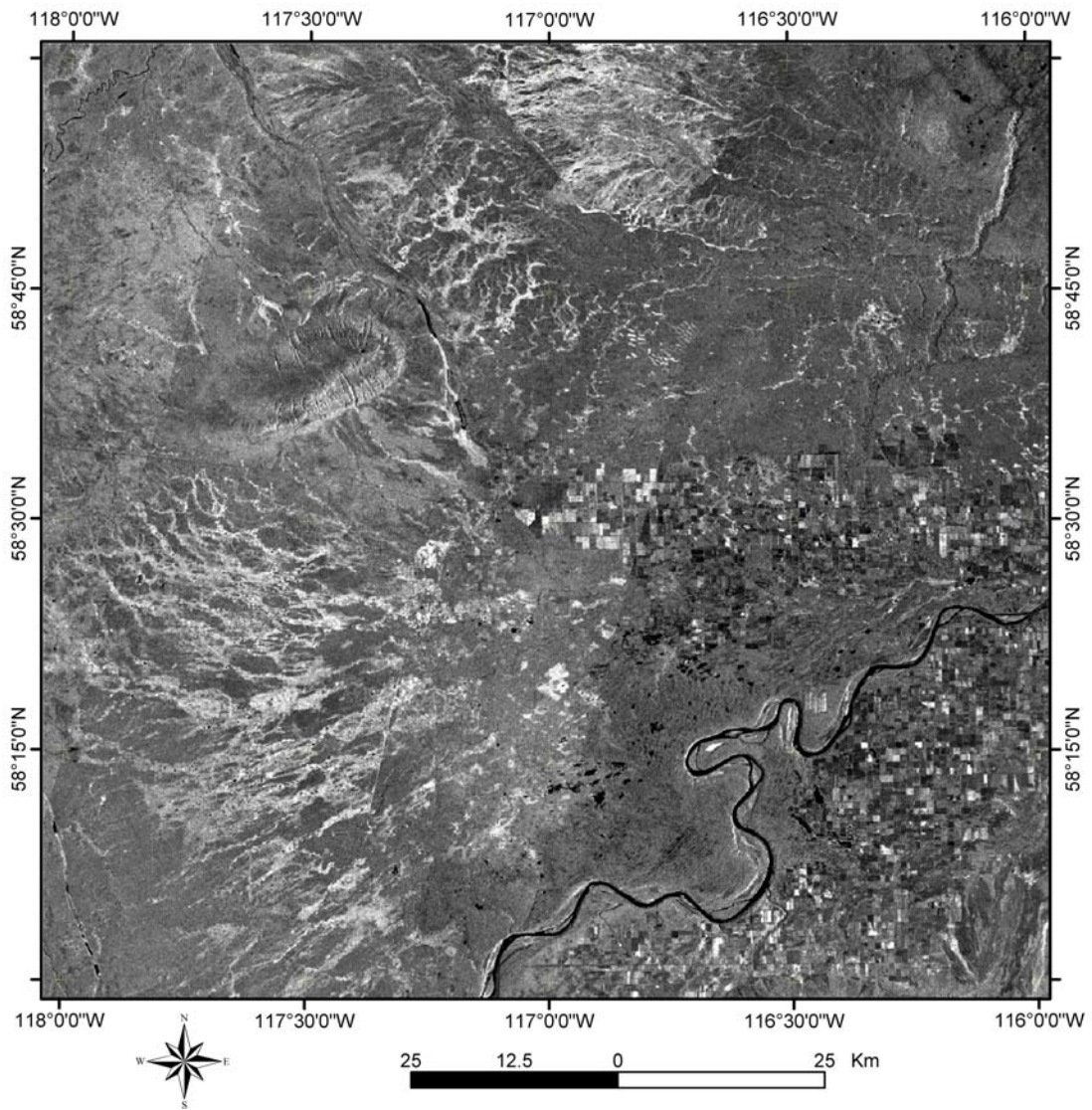


Figure 9. RADARSAT-1 Standard Beam 1 descending pass image (S1D) with an enhanced frost removal transformation using a 9 x 9 kernel.

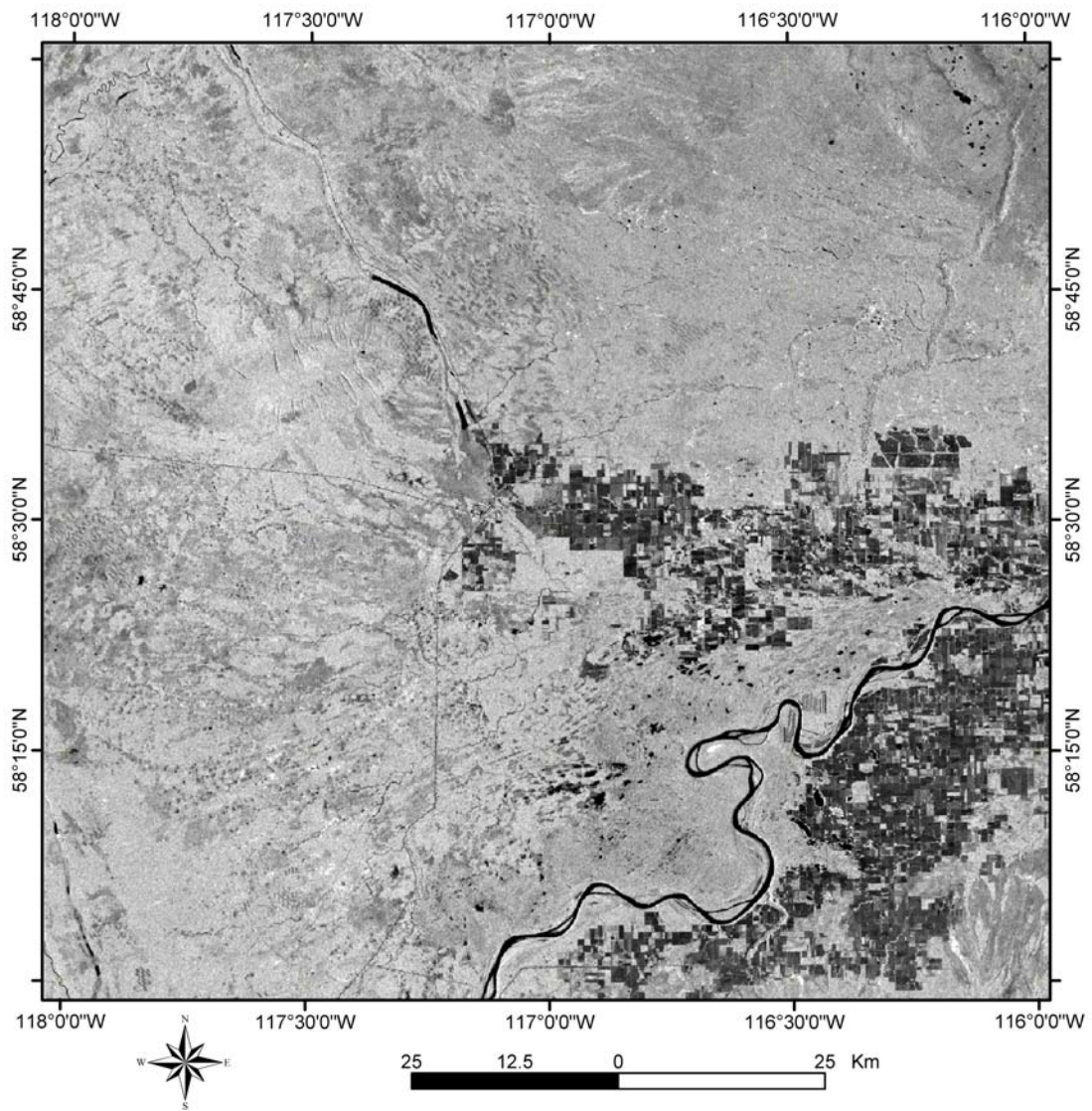


Figure 10. RADARSAT-1 Standard Beam 7 ascending pass image (S7A) with an enhanced frost removal transformation using a 9 x 9 kernel.

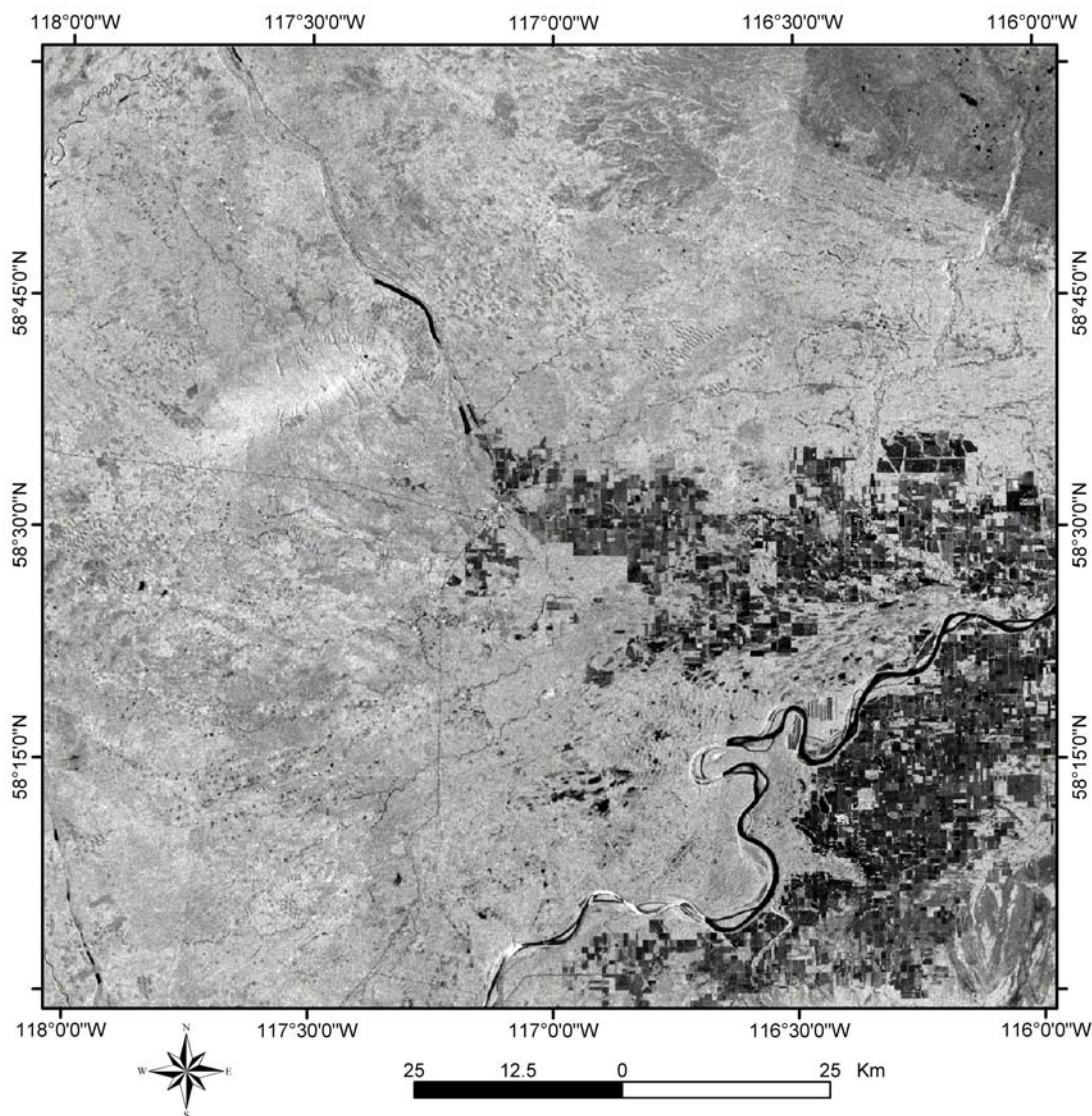


Figure 11. RADARSAT-1 Standard Beam 7 descending pass image (S7D) with an enhanced frost removal transformation using a 9 x 9 kernel.

Principal-component analysis (PCA) is a statistical method that evaluates correlation among the signals from the S1A, S1D, S7A and S7D image data and generates resultant principal-component images. It is a linear transformation that rotates the axes of image space along lines of maximum variance. The rotation is based on the orthogonal eigenvectors of the covariance matrix generated from a sample of image data from the input channels. The output from this transformation is a new set of image channels containing the principal-component images.

The covariance eigenvectors were determined by RGI using a 10 000 columns by 20 000 rows window of the four beam-mode images (Table 1). The window is located at latitude 55°37'30.3879" to 57°50'36.5615"N and longitude 113°42'25.2436" to 111°33'59.8916"W, which is out of the present study area. During the PCA, the S7 ascending image was used to mask the lakes so as to remove them from the calculation of the covariance eigenvectors. The S1 ascending image was multiplied by 1.35 and the S1 descending image by 1.60, so as to match the means of the S1 and S7 ascending and descending images.

A filter (ER Mapper std_dev_1.6) was applied to each of the four beam-position images. After PCA, a value of 11 000 was added to PC3 values and 5 000 to PC4 values to bring all of the image values into a positive range. Then, the dataset was converted into unsigned, 8-bit integer format with the pixel size remaining at 12.5 m.

Table 1. Covariance eigenvectors of principal-component analysis used by Resource GIS and Imaging Ltd. (RGI).

Input Image	PC1	PC2	PC3	PC4
S1A	0.152	0.866	0.465	-0.102
S1D	0.501	0.347	-0.759	0.230
S7A	0.594	-0.275	0.451	0.607
S7D	0.611	-0.233	0.068	-0.754

The first principal-component image (PC1; Figure 12) is a combination of positive contributions from all the input images (Table 1). Areas of open black spruce and shrubby and grassy wetlands appear as bright areas. Flat areas, such as farmlands and lakes, show up as darker tones. Areas of forested terrain, including closed aspen, closed pine and open deciduous vegetation, are displayed in mid-range tones with variable texture. Disturbed terrain, such as farmland, logged areas and roads, are highly visible as darker tones.

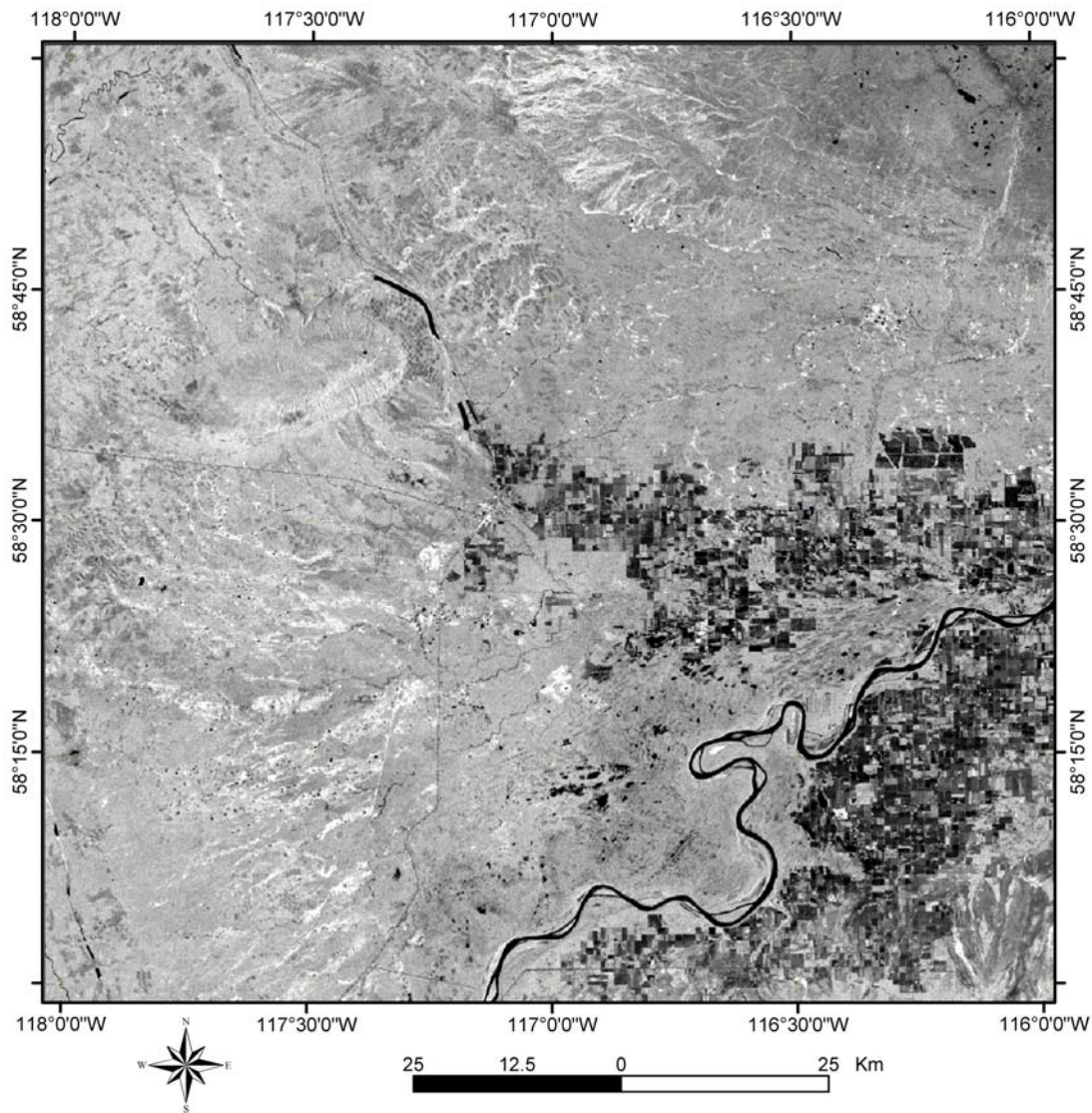


Figure 12. Principal-component 1 image for 84K processed by Resource GIS and Imaging Ltd. (RGI).

The second principal-component image (PC2; Figure 13) is characterized by positive contributions from the two S1 images and negative contributions from the two S7 images ([Table 1](#)). Thus, it represents the contrast between backscatters from the two incidence angles. As explained previously, wetlands and flat areas, including farmlands and burns, generally have a low grey value in S7 images and a much higher grey value S1 images. As a result, in the PC2 image areas of open black spruce, shrubby and grassy wetlands, and some farmlands appear as very bright areas. Areas of forested terrain, including closed aspen, closed pine and open deciduous vegetation, are displayed in dark tones with variable texture.

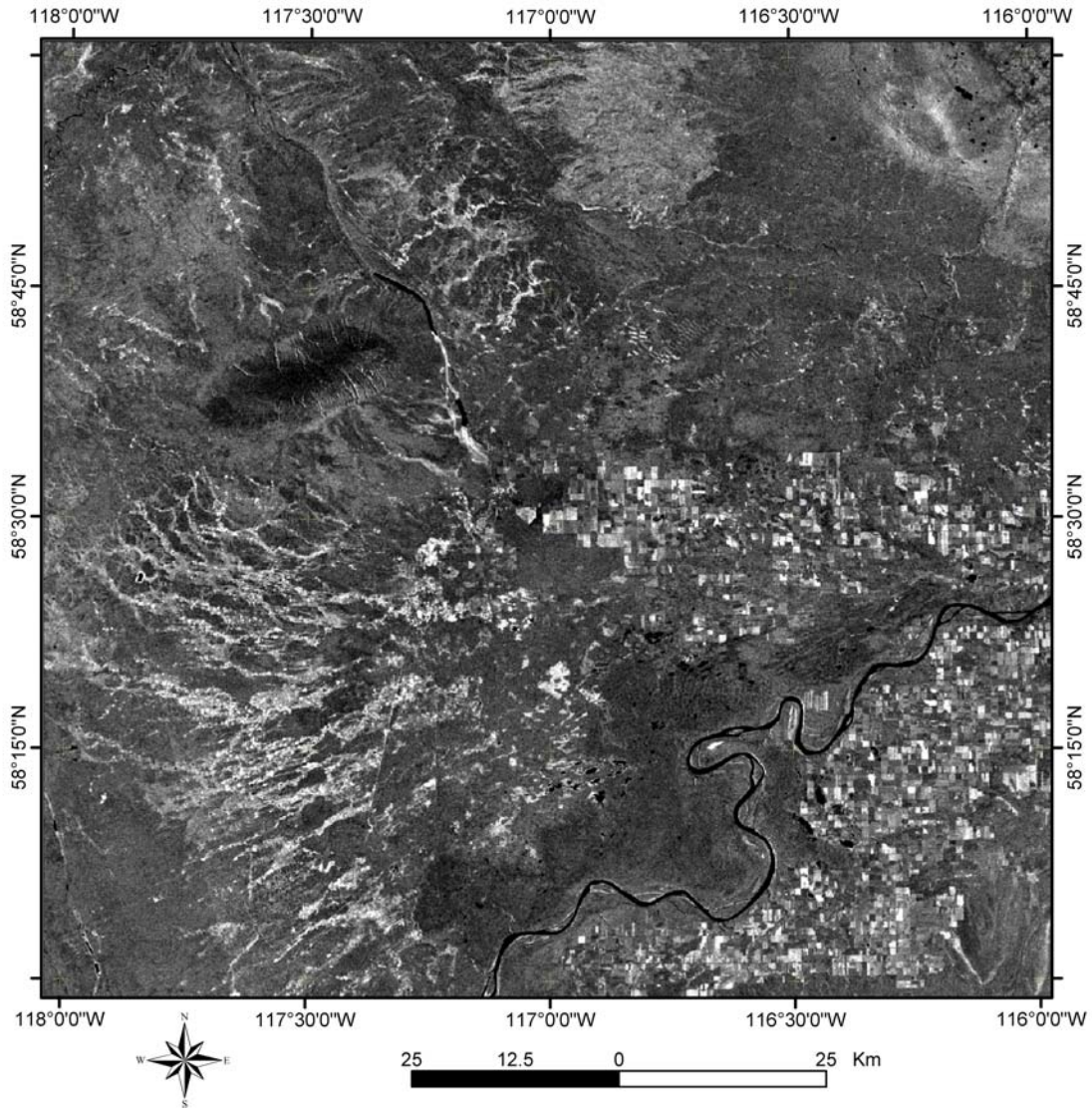


Figure 13. Principal-component 2 image for 84K processed by Resource GIS and Imaging Ltd. (RGI).

The third principal-component image (PC3; Figure 14) appears to be dominated by positive contributions of east-looking images (S1A and S7A) and negative contribution from a west-looking image (S1D; [Table 1](#)). Thus, it represents the contrast between backscatters from the two opposite directions. It presents a sunshade relief effect and highlights surficial topographic features. This is due to the fact that the slope facing the sensor tends to result in a higher radar backscatter and the slope facing away from the sensor in a low radar backscatter; thus, the contrast between the look directions contributes to an enhanced sunshade relief effect. Grunsky (2002b) and Mei et al. (2005) demonstrated that the discrimination of topographic features using the PC3 image is superior to any other optical commercial satellite imagery with similar spatial resolution, and areas of drumlins, sand dunes, eskers, crevasse fillings, embankments and other prominent topographic features typically are more clearly shown on PC3 images than on the other PCA images.

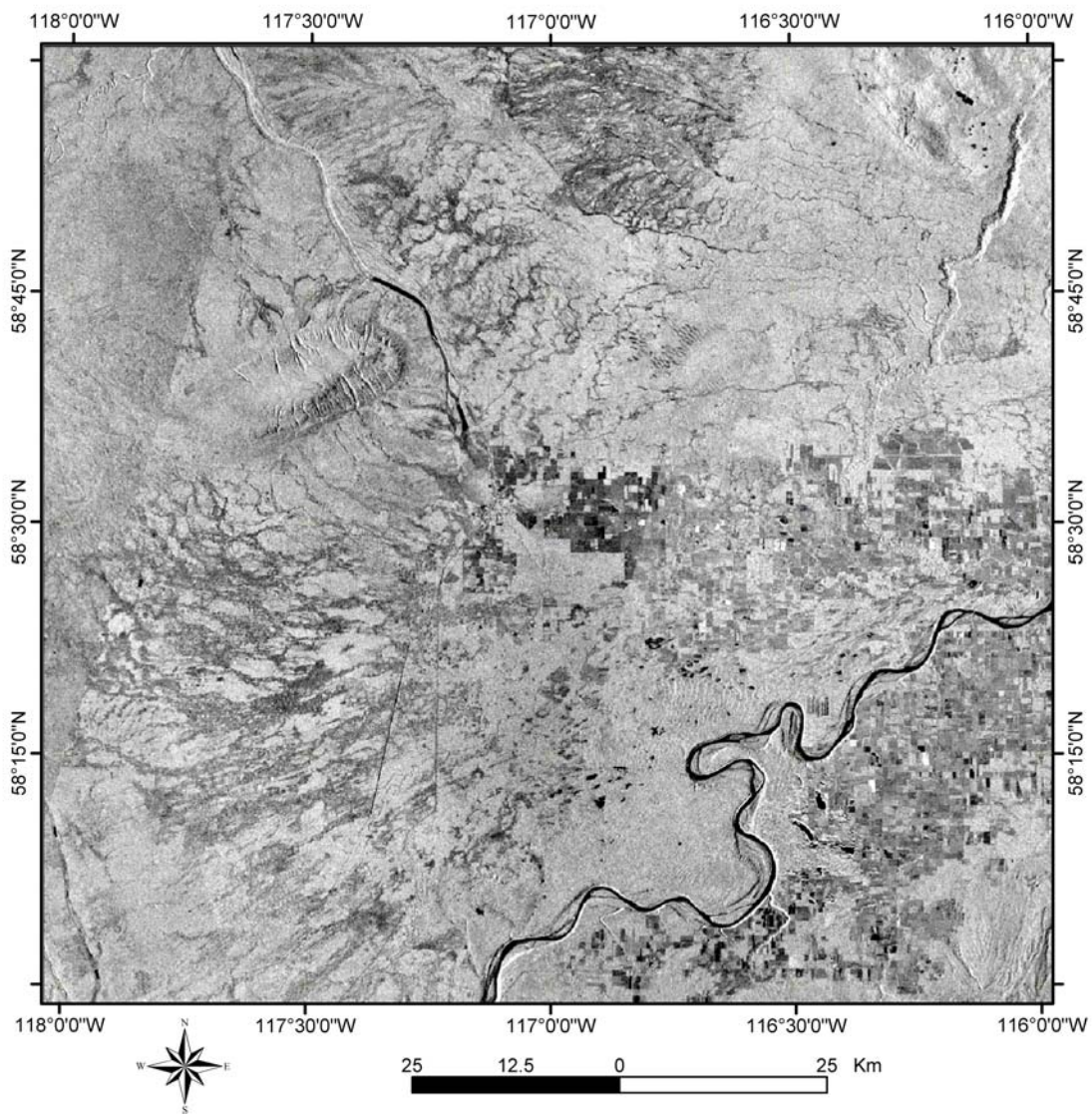


Figure 14. Principal-component 3 image for 84K processed by Resource GIS and Imaging Ltd. (RGI).

The fourth principal-component image (PC4; Figure 15) consists of a weak negative contribution from S1A, a weak positive contribution from S1D, a strong positive contribution from S7A and a strong negative contribution from S7D. Consequently, it is characterized by the contrast between the look directions of the S7 images that is offset by the contrast between the look directions of the S1 images. Consequently, the PC4 image tends to contain much less topographic information than the PC3 image, but may contain more surface roughness information.

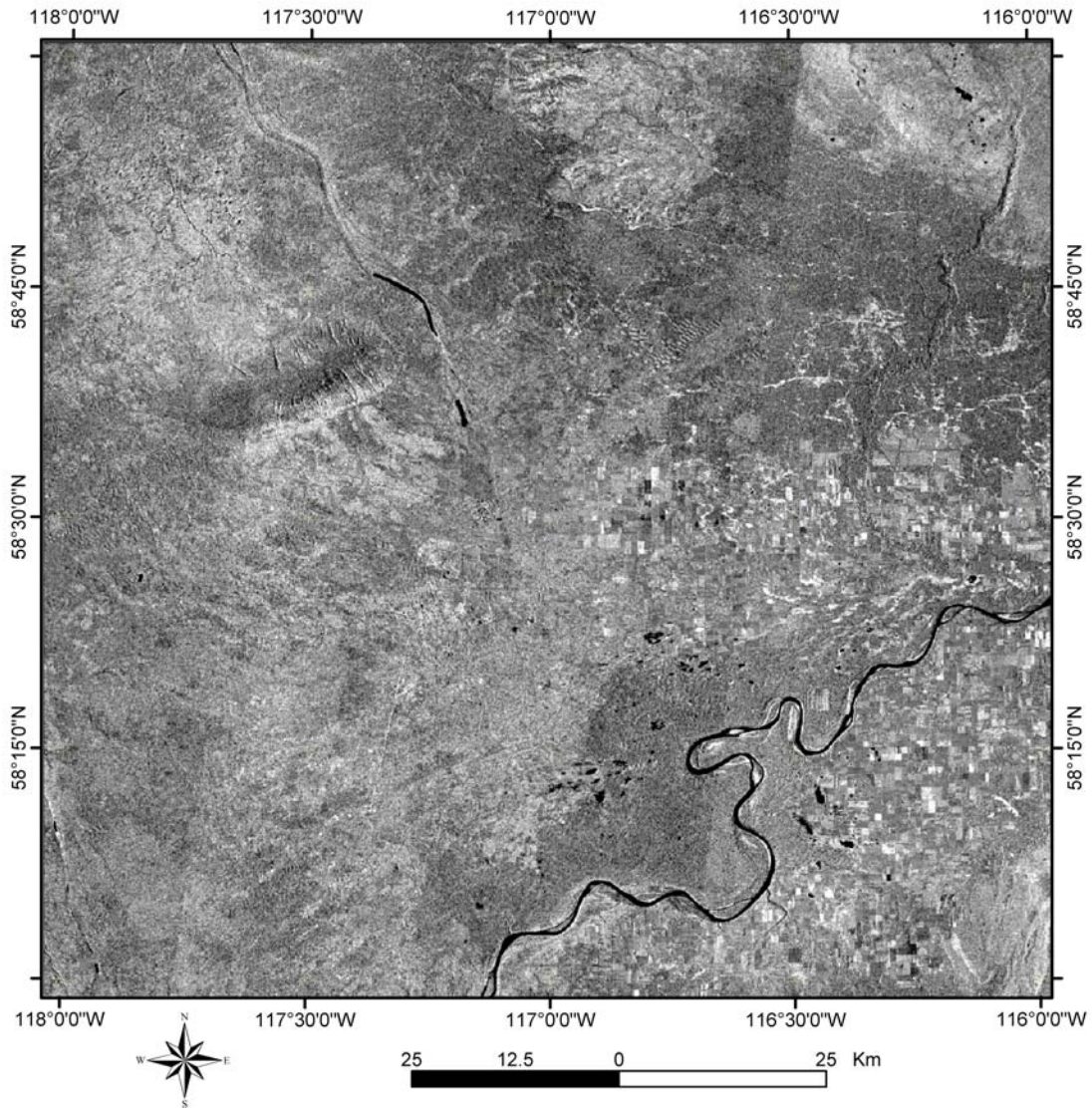


Figure 15. Principal-component 4 image for 84K processed by Resource GIS and Imaging Ltd. (RGI).

Figure 16 is a pseudocolour colour-composite image created by combining the PC1, PC2 and PC3 images. Areas of open black spruce and shrubby and grassy wetlands appear as greenish cyan, and farmlands and bedrock show as blue to purple. Areas of forested terrain, including closed aspen, closed pine and open deciduous vegetation, appear as brownish green with variable texture.

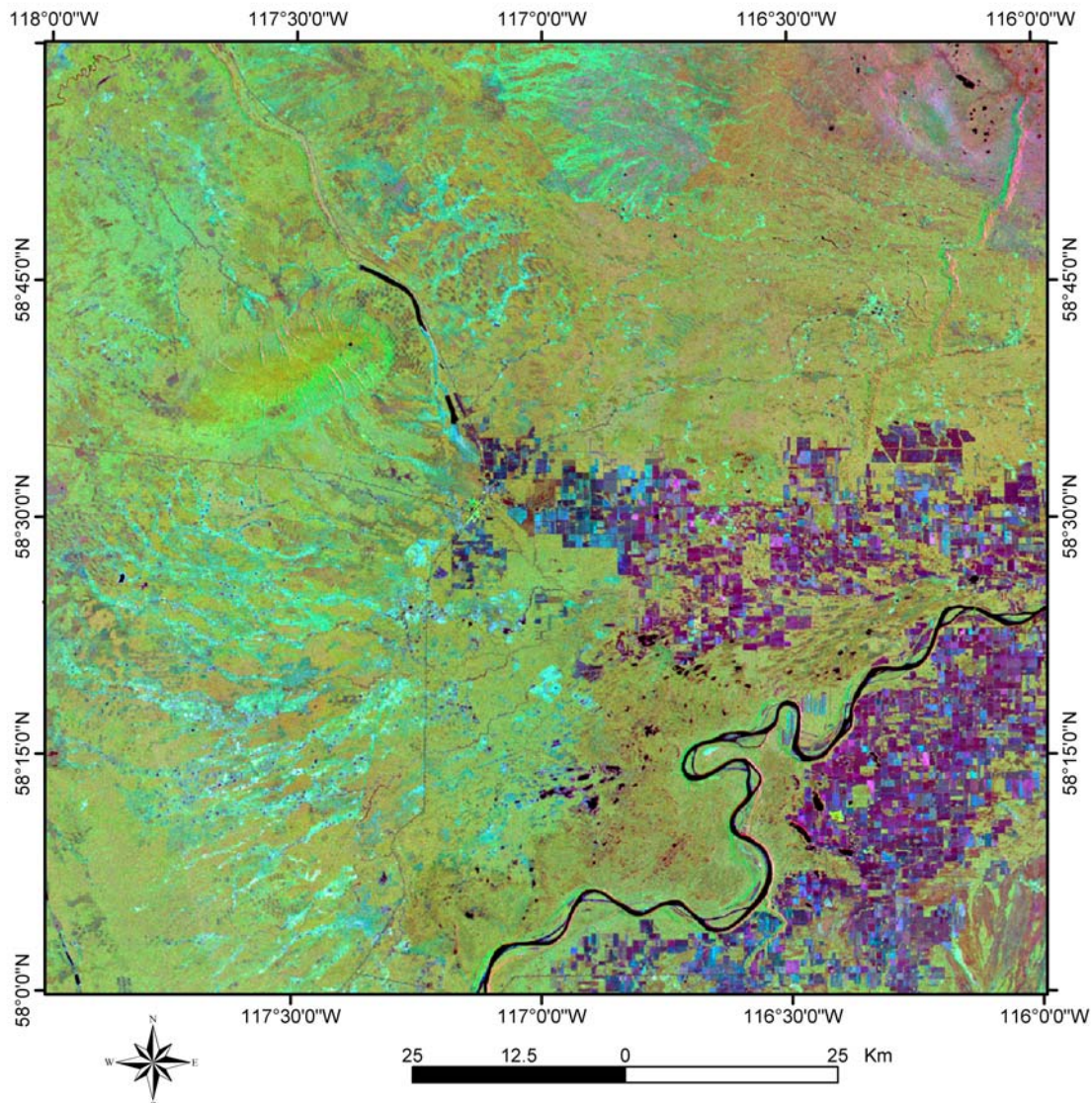


Figure 16. Pseudocolour colour-composite image with the PC3 image as red, PC1 image as green and PC2 image as blue.

4.3 RADARSAT-1 Images Processed in this Study

As mentioned previously, the existing four principal-component images processed for the study area by RGI are based on covariance eigenvectors ([Table 1](#)) that were derived from an area outside the study area. In addition, a close examination of the correlation eigenvectors used by Grunsky (2002b) and Paganelli et al. (2003), as well as covariance eigenvectors used by RGI, indicates that the contrast between the look directions in PC2 and PC3 images is often offset by one of the input images. The contrast between images

from opposite look directions can be used to highlight surficial relief, and the contrast between images from different incidence angles can be used to highlight wetland and flat areas. To maximize the contrast between the look directions and incidence angles, different linear transformations were applied to the orthorectified RADARSAT-1 images for the study area. [Figure 17](#) maximizes the contrast between images from the opposite look directions. A visual comparison to the PC3 image ([Figure 14](#)) indicates that the processed image ([Figures 17](#)) has a comparable and, in some places, even more detailed effect in highlighting topographic features. [Figure 18](#) shows the image that maximizes the contrast between images from different incidence angles. The blue areas clearly denote flat areas including wetlands, farmland, bedrock and burns. This suggests that the processed image ([Figure 18](#)) provides a comparable or even better enhancement of the wetlands than the PC2 image ([Figure 13](#)). [Figure 19](#) is a pseudocolour composite image of the two contrast images and an image created by summing up all the input RADARSAT-1 images. Land-cover types and surficial topography are well represented in this image. Areas of open black spruce and shrubby and grassy wetlands appear as cyan, and farmlands show as blue to bluish purple. Bedrock with no or sparse vegetation cover and exposed soils appear as purple. Areas of forested terrain, including closed aspen, closed pine and open deciduous vegetation, appear as green to brownish green with variable texture. A visual comparison of this image with the PCA composite pseudocolour image ([Figure 16](#)) indicates that the processed image ([Figure 19](#)) has a comparable and, in some places, even more detailed effect in highlighting various features.

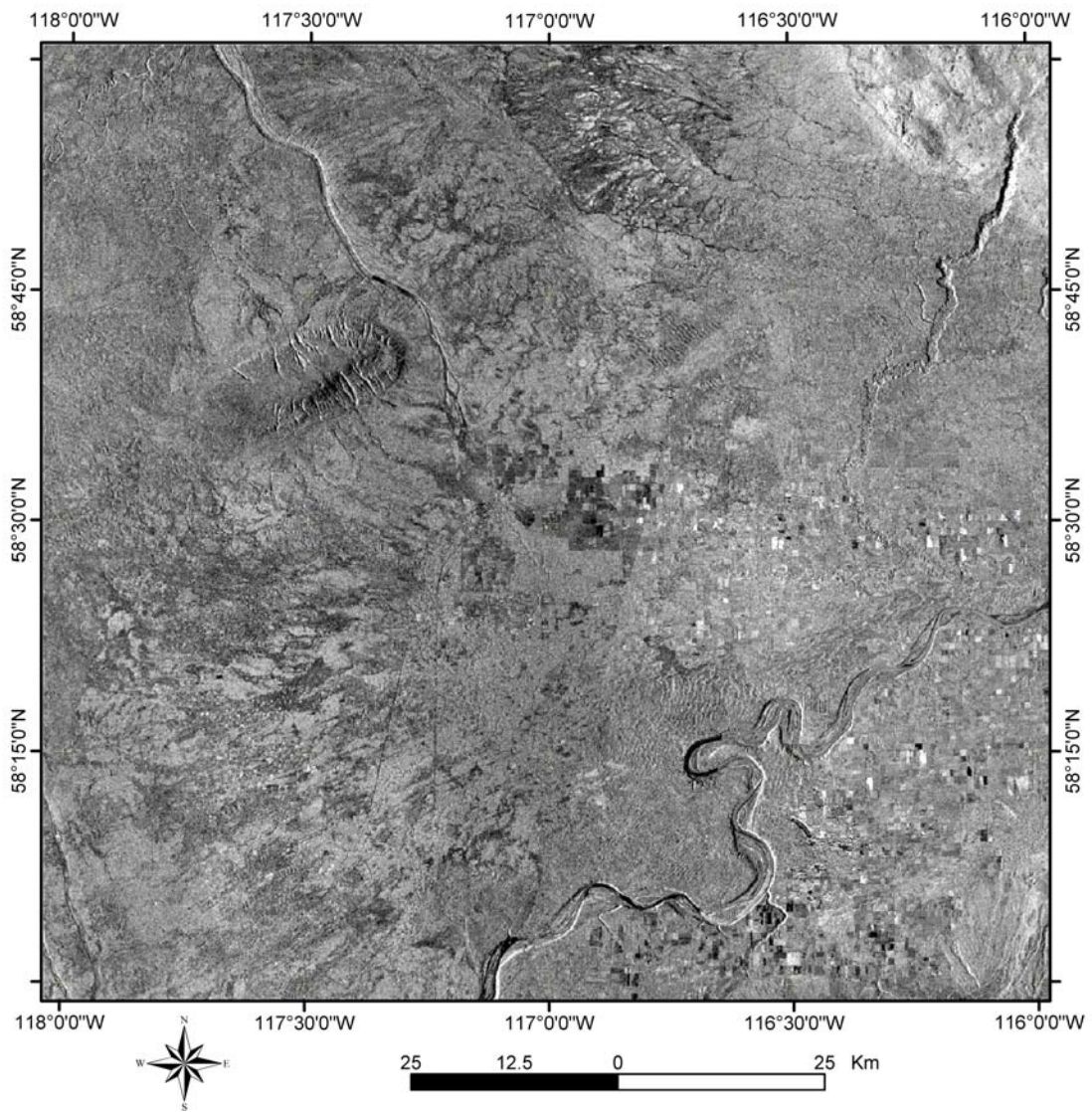


Figure 17. Image for NTS 84K created by using algorithm $([S1A + S7A] - [S1D + S7D])$.

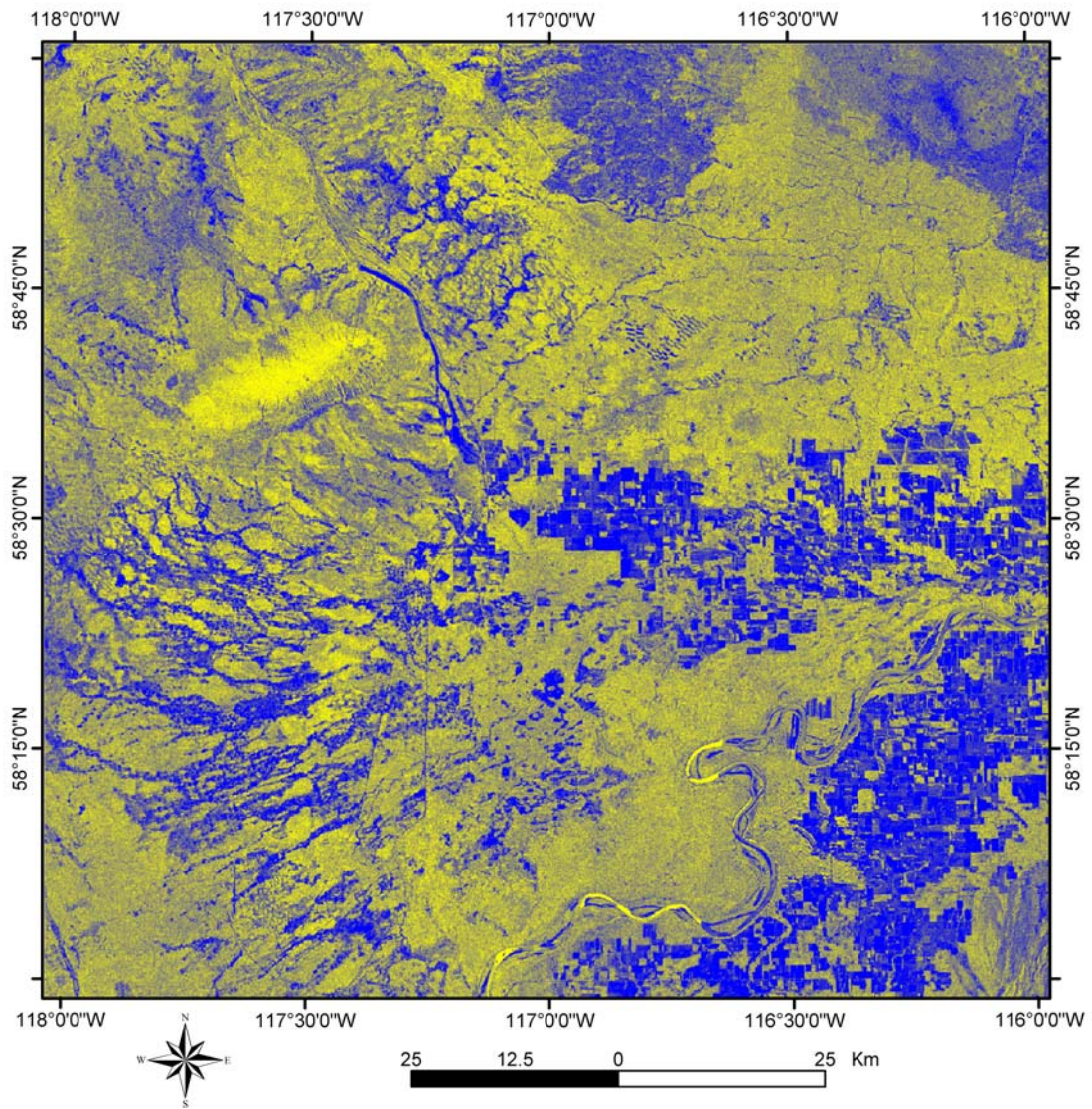


Figure 18. Image for NTS 84K created by using algorithm $([S1A + S1D] - [S7A + S7D])$. Displayed in pseudocolour.

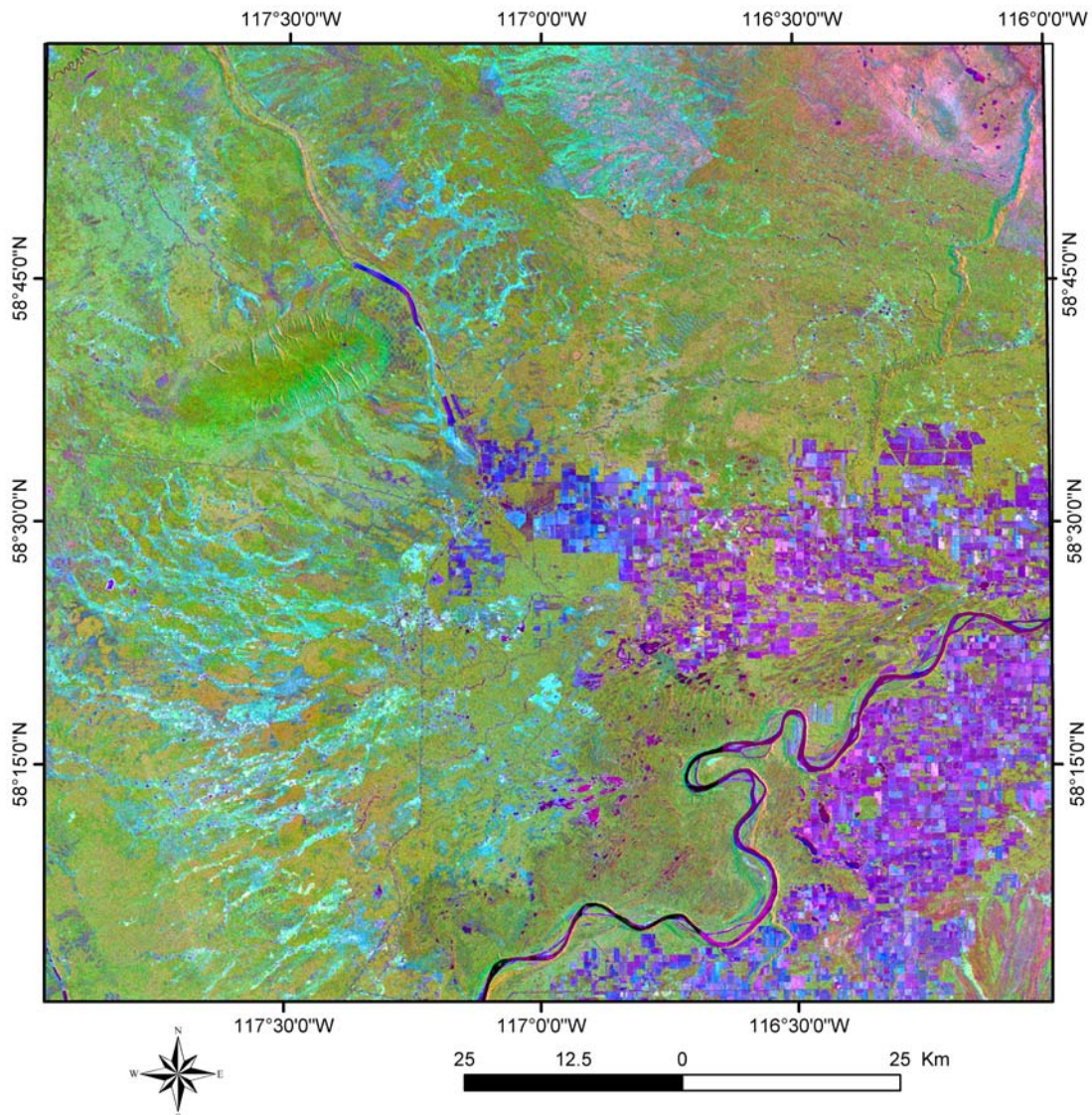


Figure 19. Image for NTS 84K created by using $([S1A + S7A] - [S1D + S7D])$ image as red, $([S1A + S7A] + [S1D + S7D])$ image as green and $([S1A + S1D] - [S7A + S7D])$ image as blue.

4.4 Digital Elevation Model from Shuttle Radar Topography Mission

The Shuttle Radar Topography Mission (SRTM) aboard the Space Shuttle ‘Endeavour’ was launched on February 11, 2000. The objective of the SRTM was to obtain elevation radar data on a near-global scale and generate the most complete high-resolution digital topographic database of the Earth to date. It generated digital topographic maps of 80 percent of Earth’s land surface (between latitudes 60°N and 56°S) at a 30 m pixel resolution. The mission objective was to produce digital topographic map products with absolute horizontal circular accuracy less than or equal to 20 m, absolute vertical height accuracy less than or equal to 16 m and relative vertical height accuracy less than or equal to 10 m. These accuracies are quoted at the 90% level, consistent with National Map Accuracy Standards of the United States (<http://rockyweb.cr.usgs.gov/nmpstds/nmas.html>). Extensive digital elevation model (DEM) data from a single source such as SRTM is especially desirable because it is consistent and comparable across large areas, whereas other high-resolution DEMs are derived from variable sources. The SRTM DEM at

30 m pixel size has been averaged into 90 m pixel size (3 arc seconds) and been made available for North and South America. The SRTM DEM data (Figure 20) for the study area, ordered from USGS website <http://seamless.usgs.gov/>, have a 50 m x 90 m pixel size after projection onto a UTM 11 map projection. A visual comparison of the SRTM DEM (Figure 20) and the processed RADARSAT-1 images (Figures 14, 17) indicates that the processed RADARSAT-1 images depict most of the surficial topographic features that can be seen in the SRTM DEM. In addition, the processed RADARSAT-1 images contain more information on land-cover type and moisture.

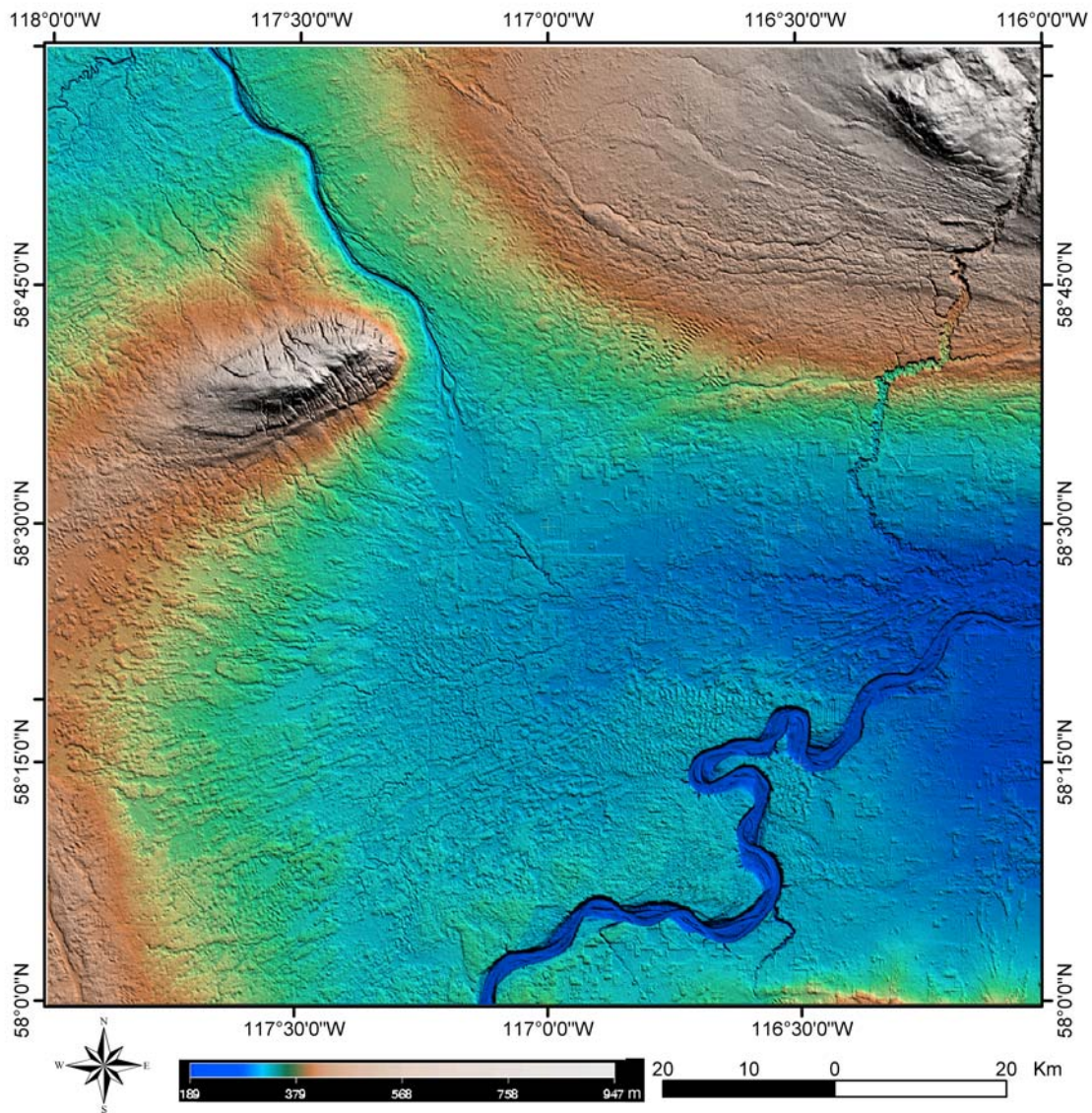


Figure 20. Shuttle Radar Topography Mission (SRTM) digital elevation model (DEM) displayed in pseudocolour combined with sunshade relief with a 45° light-direction azimuth and a sun elevation of 45°.

4.5 Landsat Image

The Landsat 7 image (Figure 21) used in the present study is a subset for the study area clipped from the Alberta mosaic of Landsat 7 Enhanced Thematic Mapper (ETM) Plus, which was produced by Photosat Information Ltd. The Landsat 7 image is a natural-colour mosaic image compiled from cloud-free images taken in the summer of 2001 and sharpened with panchromatic band (15 m resolution). The component images were then resampled into 12.5 m pixel size. This image was used to supplement ground-truthing.

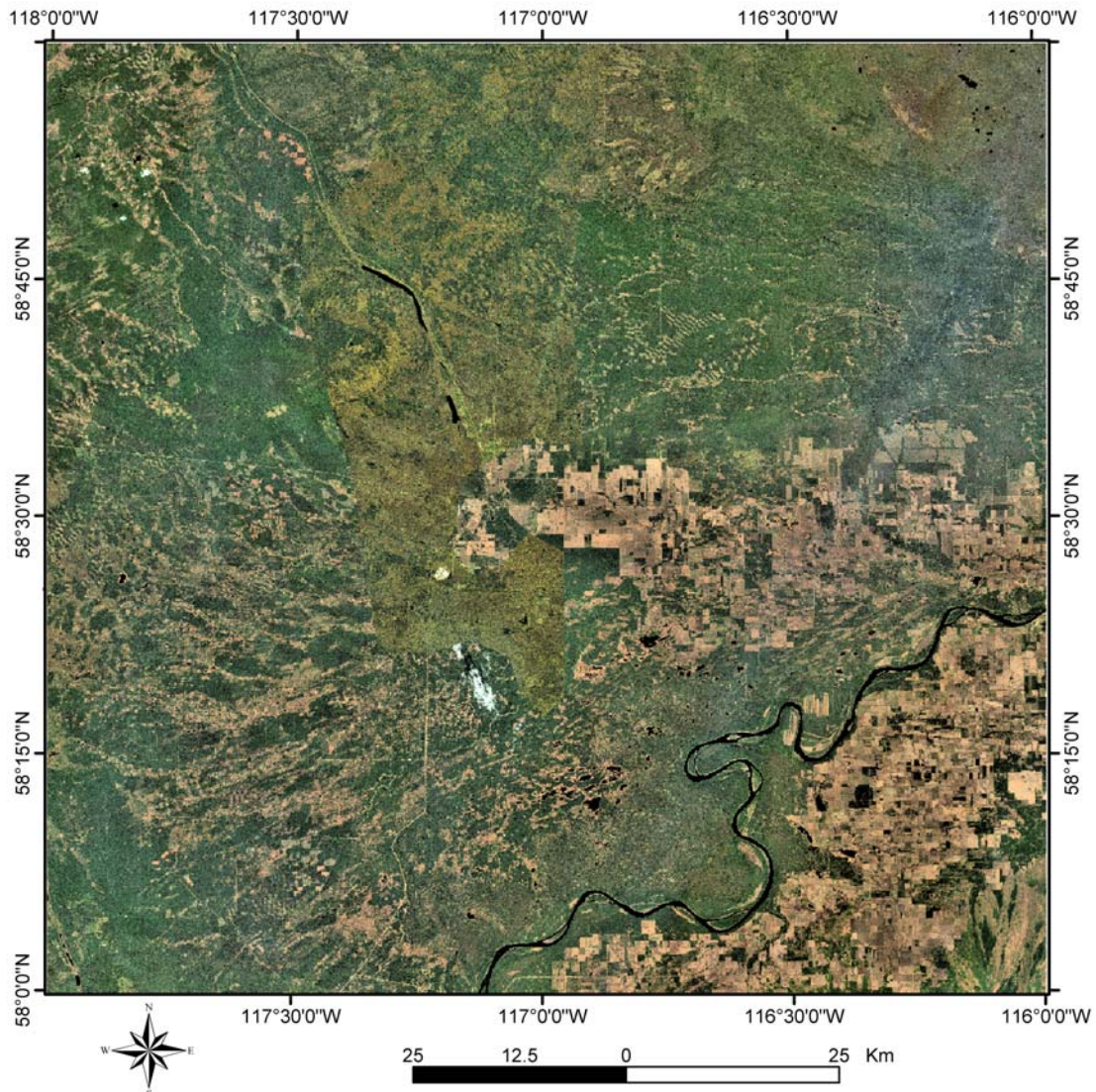


Figure 21. Landsat 7 ETM Plus image for NTS 84K.

4.6 Indian Remote-Sensing Satellite Image

The Indian Remote-Sensing Satellite (IRS) image used in the present study (Figure 22) is a subset for the study area clipped from Alberta IRS 2002 mosaic, which was produced by Photosat Information Ltd. The mosaic comprises panchromatic images taken in 1999 with a 5.8 m resolution and subsequently resampled into 5 m pixel size with the mosaic. This image was used to sharpen the Landsat 7 image to generate a higher resolution image for fieldwork planning, ground-truthing and image interpretation.

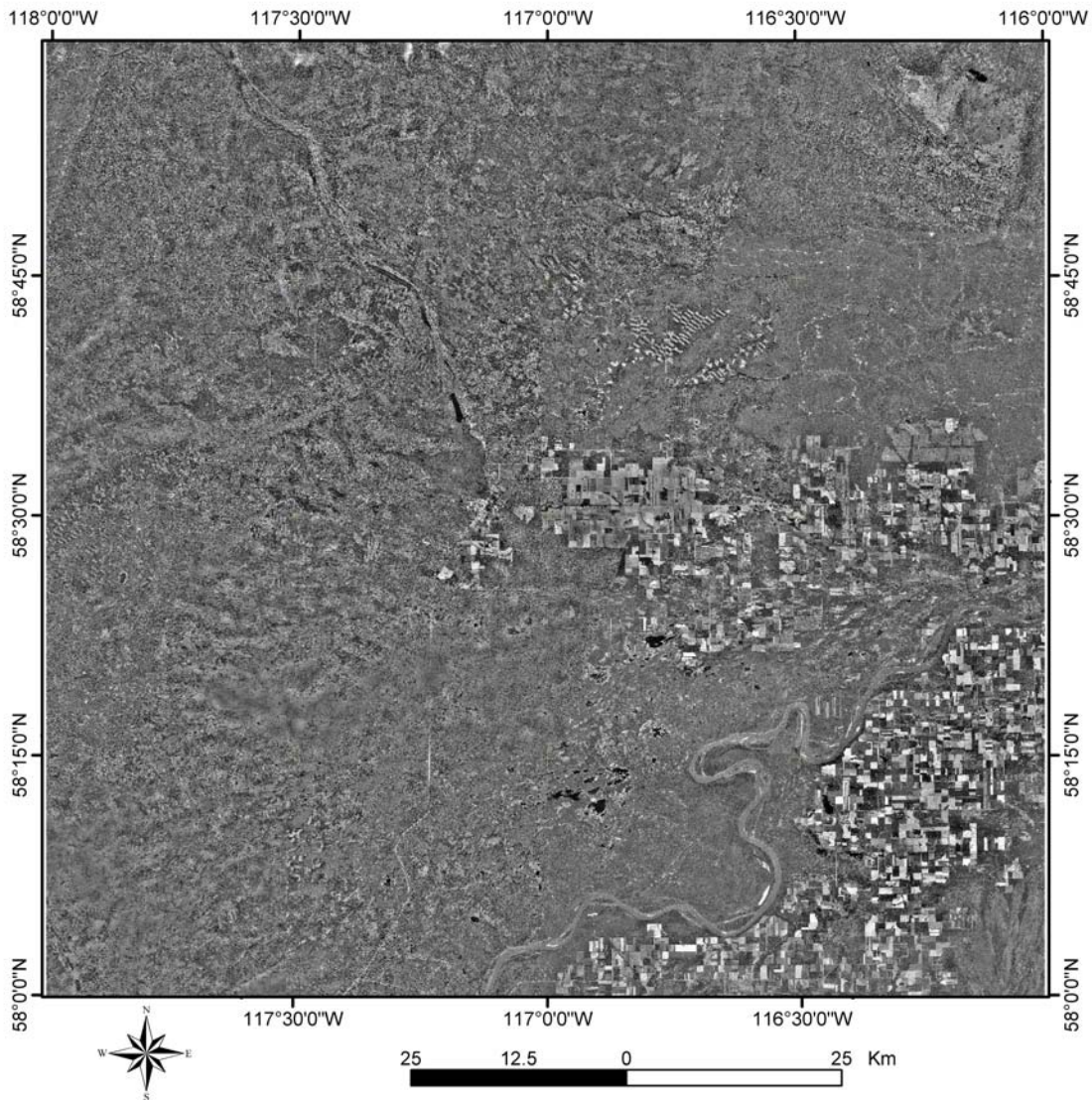


Figure 22. Indian Remote-Sensing Satellite (IRS) panchromatic image for NTS 84K.

4.7 Data Integration

The Landsat image was sharpened with the IRS image in order to raise the effective resolution to 6 m. Then, the sharpened image was fused with a shaded-relief image of the SRTM DEM to obtain a stereo effect (Figure 23). The SRTM DEM was also fused with the processed RADARSAT-1 images to acquire a stereo effect (Figures 24, 25). These processed images add a topographic effect to the features compared to Figures 19 and 21, and are therefore easier to interpret. Areas of open black spruce, shrubby and grassy wetlands, and farmlands appear as low and flat terrains, and stabilized sand dunes around the Peace River in the southeast stand out clearly. Bedrock with no or sparse vegetation cover and exposed soils can also be identified more easily. Meltwater channels, river valleys, sedimentary fans and forested terrains are more clearly displayed in the processed images that have been integrated with the SRTM DEM.

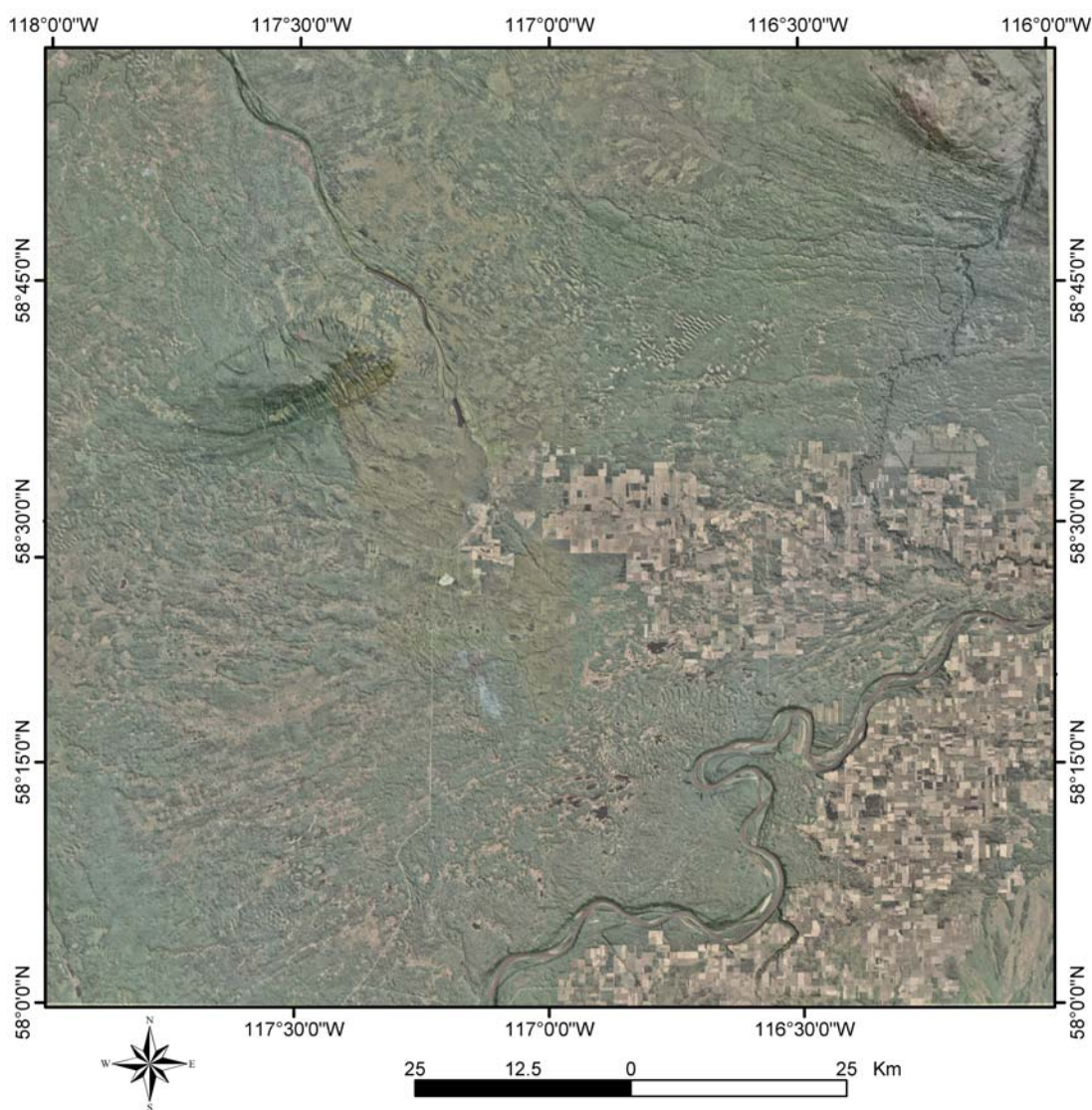


Figure 23. Image created by integration of the Landsat image, the Indian Remote-Sensing Satellite (IRS) image and Shuttle Radar Topography Mission (SRTM) digital elevation model (DEM).

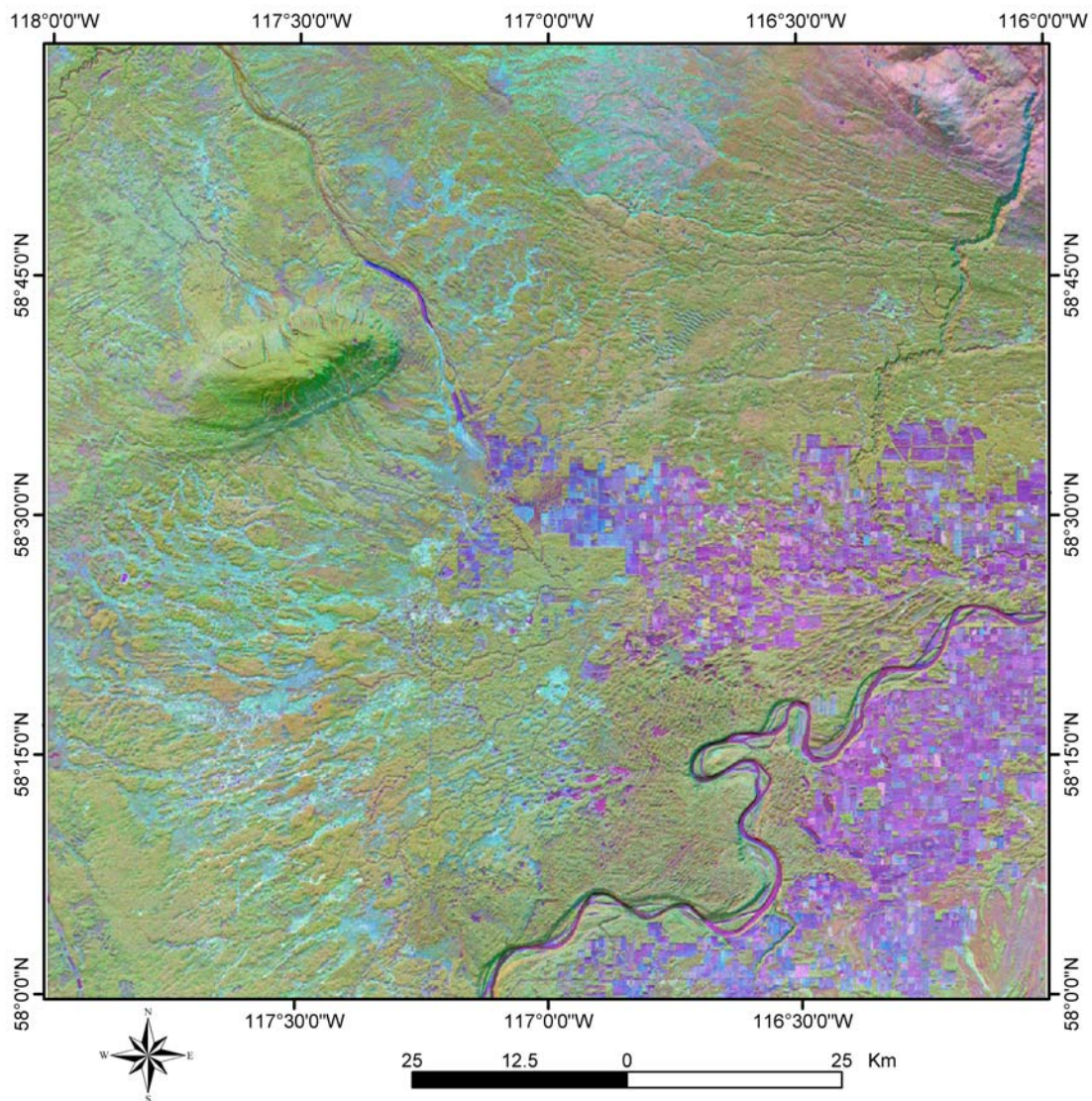


Figure 24. Image created by fusing Shuttle Radar Topography Mission (SRTM) digital elevation model (DEM) with pseudocolour composite image of processed RADARSAT-1 images, using $([S1A + S7A] - [S1D + S7D])$ image as red, $([S1A + S7A] + [S1D + S7D])$ image as green and $([S1A + S1D] - [S7A + S7D])$ image as blue.

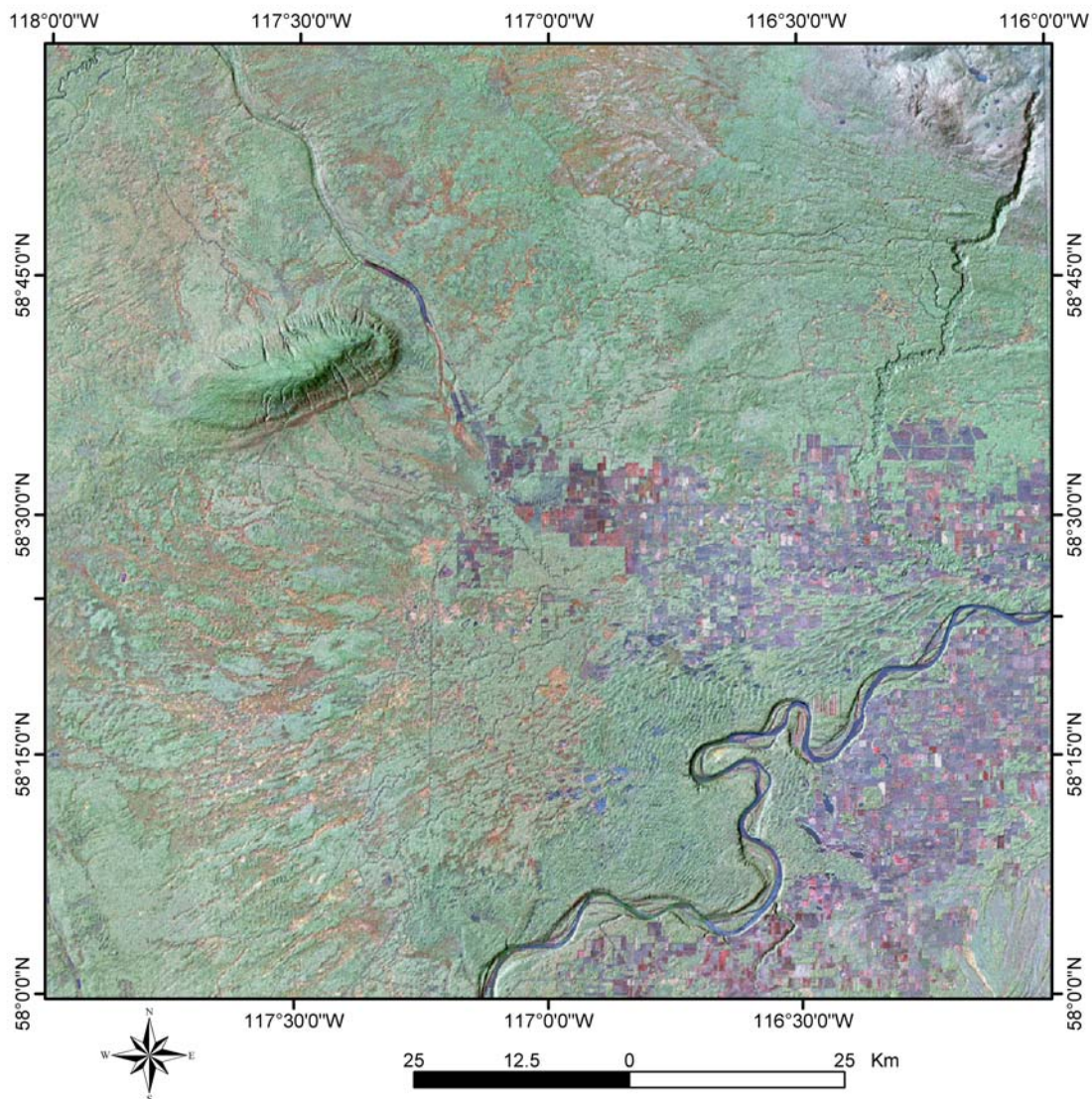


Figure 25. Image created by fusing Shuttle Radar Topography Mission (SRTM) digital elevation model (DEM) with pseudocolour composite image of processed RADARSAT-1 images, using $[(S1A + S7A) - S7D]$ image as red, $[(S1A + S7A) - S1D]$ image as green and $[(S1A + S7A) / S7D]$ image as blue.

5 Interpretation and Results

Previous knowledge, obtained from publications (Fox et al., 1987; Smith et al., in press) and AGS surficial mapping of the adjacent map areas (Plouffe et al., 2004; Paulen et al., 2005a, b; Smith et al., 2005), has proven to be crucial in interpretation of the processed images. It has been well established that, between 11 500 and 11 000 yr. BP, proglacial lakes developed in the Fort Nelson Lowland in the northwest and the Fort Vermilion Lowland (Peace River Lowland) in the central and southeast (Lemmen et al., 1994; Dyke et al., 2003). As a result, fine glaciolacustrine sediments were deposited above the ubiquitous till deposited by the late Wisconsin glacial advance. After the retreat of the Laurentide Ice Sheet and drainage of the proglacial lakes, sand dunes formed in the early Holocene, and organic and alluvium deposits were initiated and continue to develop to this day. Holocene incision by rivers has resulted in colluvial deposits developing along rivers and slopes.

The interpretation of the surficial geology presented in this report was also augmented by limited ground-truthing that was conducted in August 2004. The sites investigated are shown in Figure 26 and listed in [Appendix A](#), together with information on vegetation, geomorphology, inferred genesis, material type and other comments.

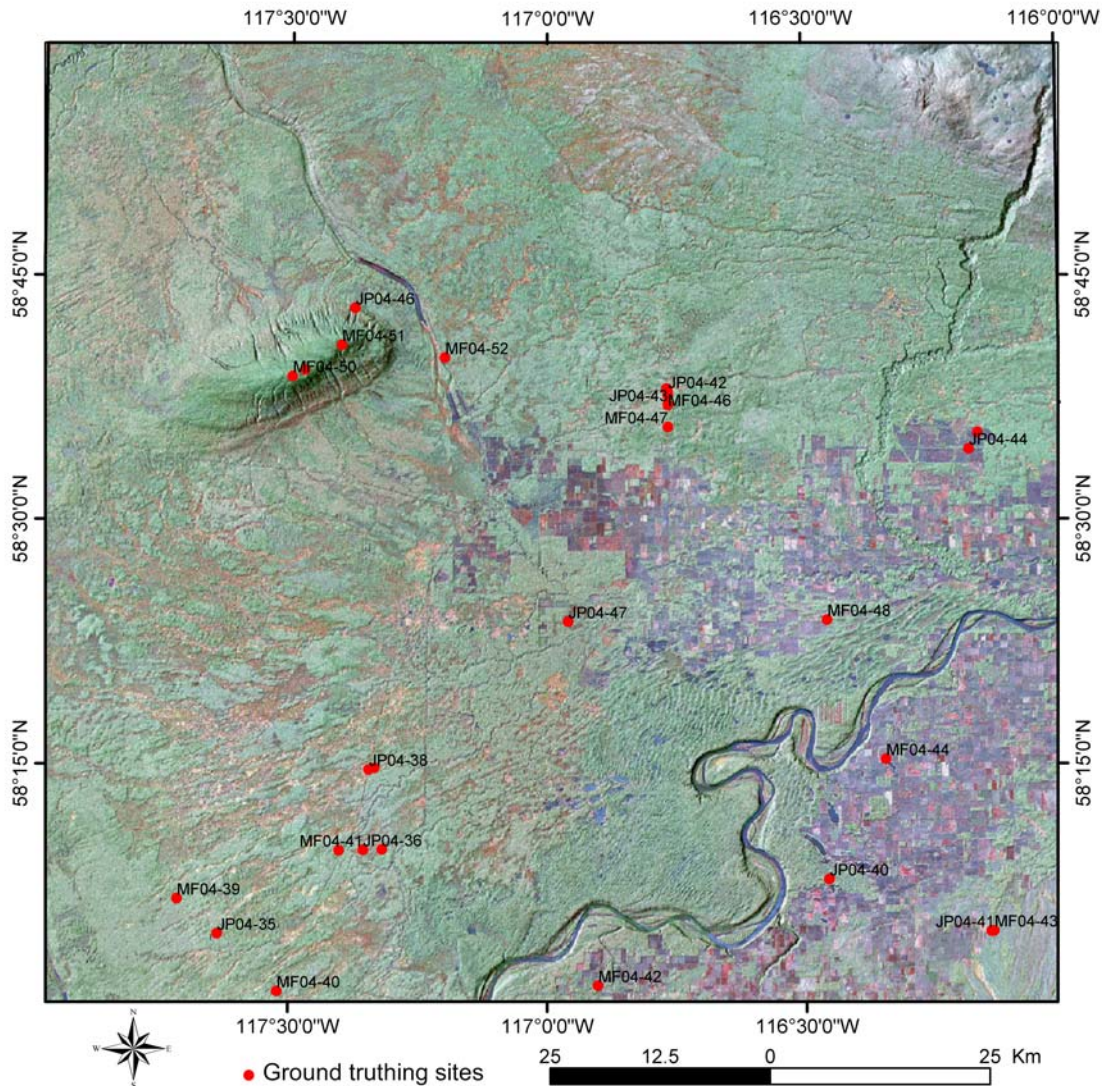


Figure 26. Ground-truthing sites shown on the processed RADARSAT-1 image, with $[(S1A + S7A) - S7D]$ image as red, $[(S1A + S7A) - S1D]$ image as green and $[(S1A + S7A) / S7D]$ image as blue.

On the processed SRTM DEM images ([Figures 1, 4 and 20](#)), the Fort Nelson Lowland in the northwest and the Fort Vermilion Lowland (Peace River Lowland) in the central and southeast are generally flat with low relief, with the Mount Watt and Caribou Mountains highland situated between them. The highlands and the retreating ice margin blocked glacial meltwater drainage and mantled the lowlands with thick glaciolacustrine sediments (Lemmen et al., 1994). This has been confirmed by most of the ground-truthing sites located in the Fort Vermilion Lowland (*see* [Appendix A](#) and Figure 26).

Peatlands are clearly shown on the processed RADARSAT-1 images (e.g., [Figures 16, 18, 19, 24 and 25](#)) and sand dunes stand out visibly on all the processed images. In Figure 26, for example, site JP04-38, like many other sites in the lowland, confirms that the greenish areas, except in the sand dune field, are mostly

poplar forest stands underlain by glaciolacustrine deposits (see [Figure 26](#) and [Appendix A](#)). Nearby, site JP04-39 (not labelled because it was too close to JP04-38) confirms that the brownish areas are peatlands with organic material overlying the glaciolacustrine deposits. Sites JP04-40 and MF04-48 confirm the assignment of the sand dune field from the processed images. Two subregions can be recognized from the processed images: the southwestern part of the sand dune field displays a well-developed stabilized field of dunes, whereas the northeastern part demonstrates a less mature dune field dominated by separated sand dunes that are suspected to have been reworked during Holocene droughts (Wolfe, 2002).

Alluvial fan-like features are also clearly shown around Mount Watt and on the northern slope of the Buffalo Head Hills. Site MF04-43 is located in a wetland dominated by sphagnum and willows. At this site, two units were recognized beneath a 30 cm thickness of black organic material. The upper unit is about 1.7 m thick and consists of clayey silt with some very fine sand; the lower unit is a layer of firm clayey silt that can be assigned a glaciolacustrine origin. The two units have a sharp contact, suggesting that the upper unit was probably washed down the Buffalo Head Hills and deposited in the shallow margin of glacial Lake Peace. It should be noted, however, that a rapidly shallowing (regressing) glacial lake could also have produced this feature, as was noted in the glacial Lake Hay basin (Paulen et al., 2004, 2005b; Smith et al., in press). Site JP04-41, which is 300 m west of site MF04-43 and located within a poplar stand, is underlain by a layer of glaciolacustrine silt and a layer of silty clay below. This may suggest that this is a subaerial fan with early Holocene resedimented (slope wash) material.

As shown in the SRTM DEM images in [Figure 3](#), as well other processed images (e.g., [Figures 20, 23–25](#)), numerous parallel meltwater channels developed in the northeastern part of the study area. Limited road access prevented ground-truthing of this area. To the southwest of this area, subtle flutings can be seen from the processed images. Site MF04-52 is located in the southwest margin of this fluted area, and till occurs at surface. At the extreme southern margin of these areas with flutings and meltwater channels, sites MF04-49 and JP04-44 revealed the presence of till. These three sites, together with the processed images, strongly suggest that the northeastern part of the study area, which contains the flutings and meltwater channels, is underlain by till.

It was found that the processed images cannot be used to precisely delineate the boundaries between surficial materials, except that the boundaries of peatlands, eolian sand fields and alluvial fan-like features that can be easily distinguished from the processed RADARSAT-1 images. The glaciolacustrine plain is represented by low and flat to gentle topography, overlain by extensive wetlands and farm lands, and the area with till can generally be differentiated from the glaciolacustrine deposits by such characteristic textures as flutings, meltwater channels and hummocky topography. Nevertheless, the boundary between the glaciolacustrine and till deposits is not distinct on the processed images. This may be explained partly by the fact that the till surface was bevelled by water along the glacial lake shorelines, including an ice margin on the eastern boundary. As a result, sites M04-39, M04-47 and JP04-43 revealed material that is water-laid diamicton deposited under, at or adjacent to the retreating ice margin, which confined the proglacial lake between the highlands.

Adding to the complexity are numerous streams on the flat lowland. Site JP04-47 revealed that a 1.8 m thick layer of sand is underlain by a layer of glaciolacustrine clay with a sharp contact. The processed images show that this site is located near an intersection of two creeks. It is difficult to determine whether this layer of sand represents fluvial sand or vegetated sand dunes. Based on the observation that the farmland mainly extends along the margins of former glacial Lake Peace, this sand is likely shallow water (littoral) glaciolacustrine sand.

The processed images also show some patterns that would not have been recognized by field observation alone, as the imagery provides a synoptic view of the study area. The processed satellite image in [Figure 27](#) shows a finger-print-like structure on the farmland in the southeast corner of the area. Aerial photographs also show this surface morphology. Ground observation reveals that this area is represented

by swell-and-swale topography with about 2 m of relief. Field observations in the swale from site MF04-44 reveals that this area is characterized by a 2 m thick layer of well-sorted, very fine sand underlain by rhythmically bedded glaciolacustrine silt and clayey silt. It could not be determined in the field whether this layer of sand represents eolian sediment or glaciolacustrine littoral deposits (e.g., point bars or beaches). The pattern on the satellite image suggests that this area probably represents an old point bar that was probably reshaped by eolian processes in the early Holocene. The pattern of ridging, however, appears to be concave away from the Peace River valley. Faint ridging patterns such as these have been observed in the Peace River valley to the south (Henderson, 1959; Paulen, 2004) and near the Fort St. John area of British Columbia (Vic Levson, pers. comm., 2004), and are attributed to slight downslope movement of water-saturated glaciolacustrine clay in the newly drained glacial Lake Peace basin (Paulen et al., 2003).

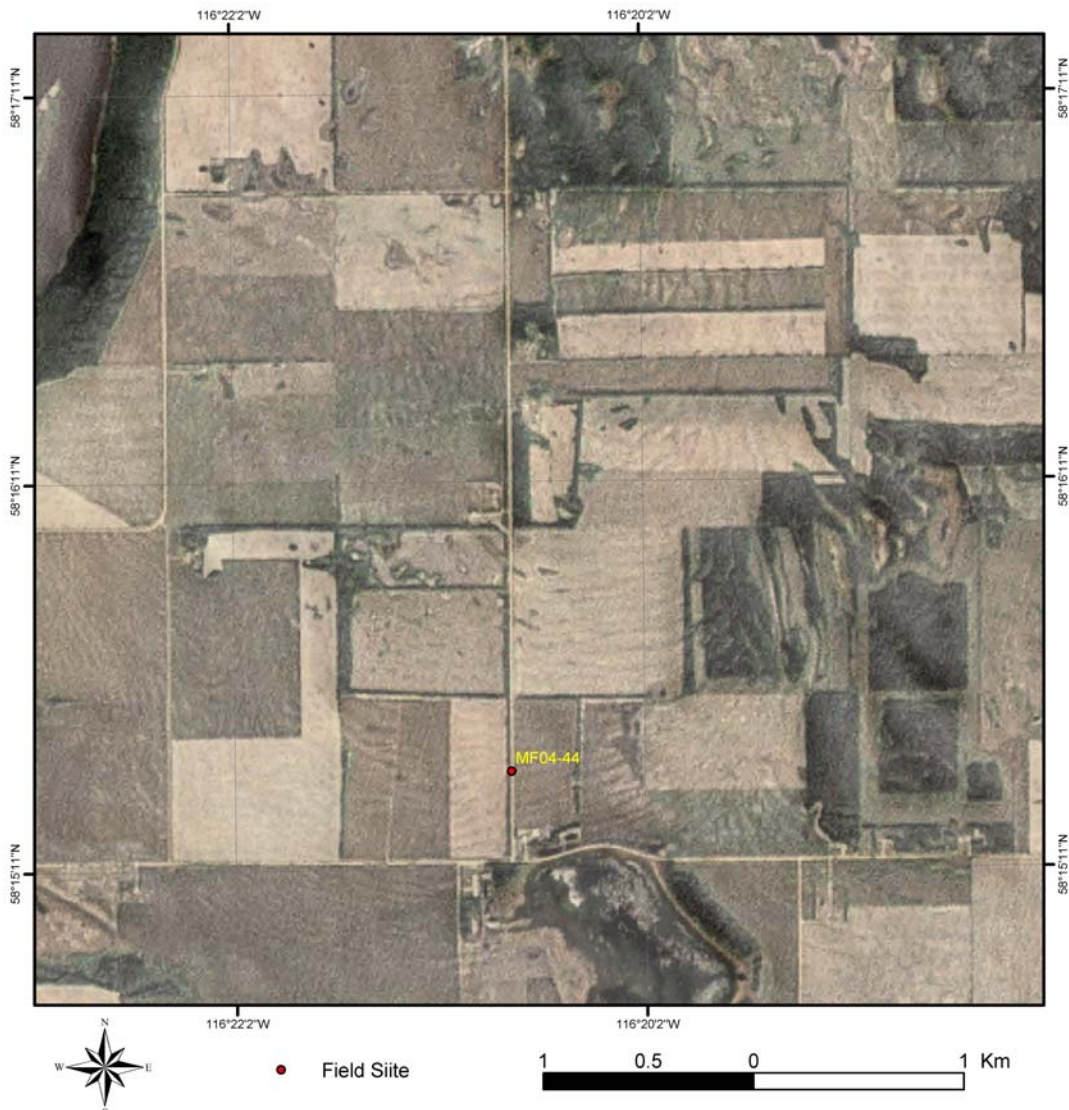


Figure 27. Finger-print-like ridges on a portion of the processed image in [Figure 23](#) around field site MF04-44.

Figure 28 reveals an area with a dimpled pattern on the satellite image. Ground observation confirms that this area represents very low relief hummocks. Site MF04-42 reveals that this area is underlain by glaciolacustrine silty clay. Hummocks of this nature were first mapped in the Peace River valley by Henderson (1959), who described them as ‘mound swarms’. Most of these circular features noted by Henderson were formed in ice-stagnation moraine, but he did notice several areas where the mounds were formed in glacial lake silt, after the lake had drained. He attributed these to the growth of ice wedges in the water-saturated sediment during periglacial conditions (Henderson, 1959). Similar features occur in the former basin of glacial Lake Hay, where round mounds occasionally have collapsed centres (Paulen et al., 2005b). It is suspected the circular hummocks in the glacial Lake Hay basin formed by ice wedging under similar periglacial conditions (Paulen et al., 2004; William Shilts, pers. comm., 2004). The low-relief hummocks seen in the processed satellite image were very likely formed under the same conditions seen in the Peace River valley to the south and in the former basin of glacial Lake Hay, and indicate the existence of permafrost during the early Holocene, after glacial Lake Peace had drained from the region.

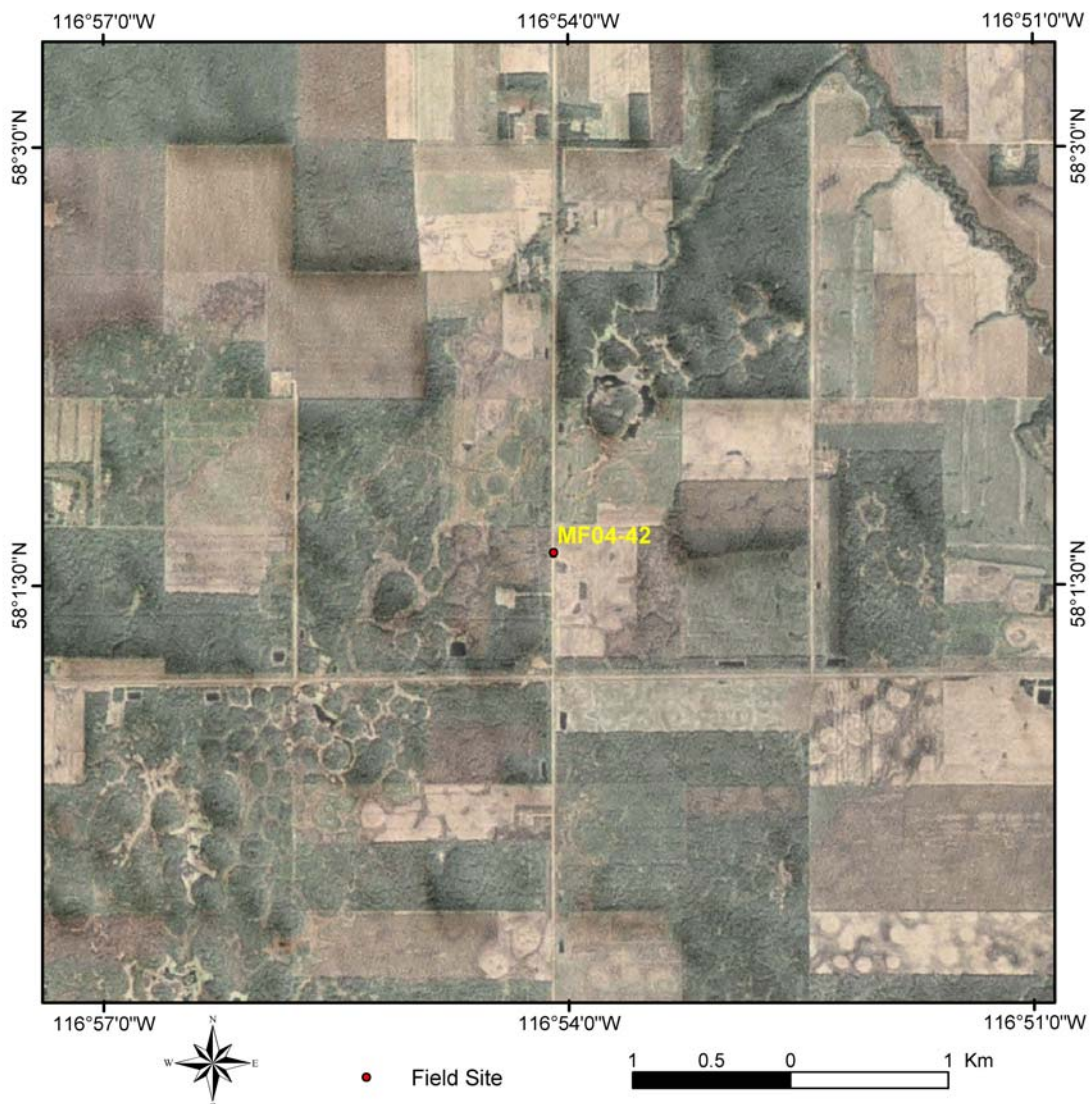


Figure 28. Polygonal dimpled pattern on a portion of the processed image in [Figure 23](#) around field site MF04-42.

The results of visual interpretation of all the processed images, augmented with limited ground-truthing, can be used to modify the NTS 84K portion of the ultra-reconnaissance map of Fox et al. (1987). The resulting map (Figure 29) provides a framework of potential surficial material distribution, for input into the actual surficial mapping of the area. The boundaries of the eolian deposits and wetlands were refined from those of Fox et al. (1987). Nevertheless, the boundaries of the major map units, including moraine, glaciolacustrine and bedrock, remain speculative.

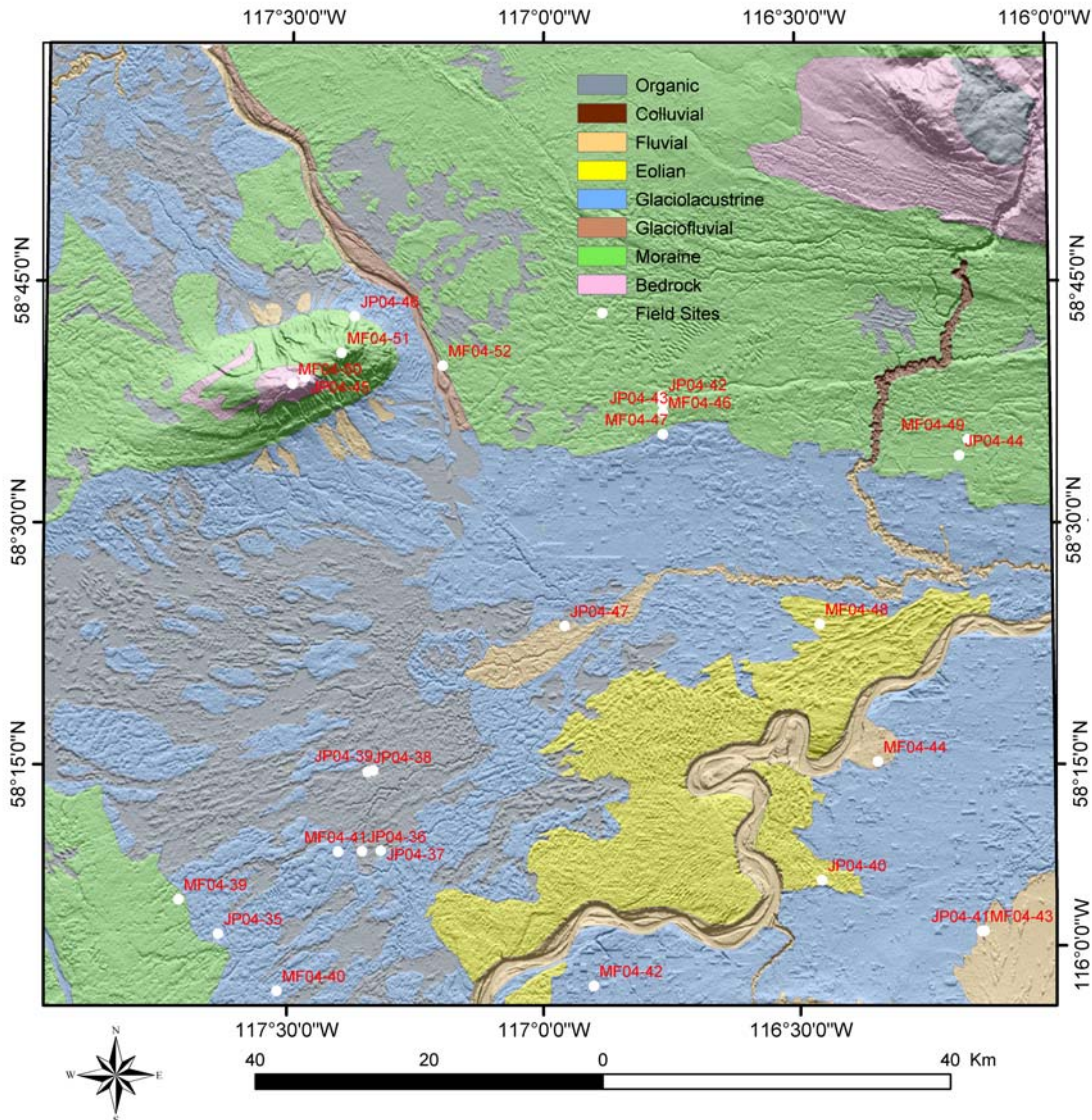


Figure 29. Interpreted surficial geological map superimposed on a shaded-relief image of the Shuttle Radar Topography Mission (SRTM) digital elevation model (DEM). Surficial materials and their boundaries were modified from Fox et al. (1987) by using remote-sensing imagery supplemented with field observations.

6 Discussion and Conclusion

In general, the addition of remote-sensing data will increase the information available to the geologist who is creating the surficial map and enhance understanding the geological history of the area. Remote-sensing data will not, however, reduce the resources required, because the most expensive aspect of surficial mapping is the ground-truthing that must be undertaken regardless of the availability of these data.

The present study indicates that topographic and geomorphological information can be extracted from RADARSAT-1 Standard Beam 1 and 7 images in both ascending and descending passes, by utilizing simple algorithms to contrast the difference between images from the different looking directions. In addition, wetland information can be extracted by using simple algorithms to contrast the difference between images from different incidence angles. Using RADARSAT-1 images can also help to identify characteristic glacial features, including flutings, meltwater channels and hummocks, as well as alluvial deposits and sand dunes. RADARSAT-1 images of multiple beams are very useful in wetland mapping of northern Alberta.

The combined use of remotely sensed data, including RADARSAT-1 images, Landsat, Indian Remote-Sensing Satellite (IRS) and Shuttle Radar Topography Mission (SRTM) digital elevation model (DEM), enhances preliminary mapping of surficial material in northwestern Alberta. Landsat images sharpened with the IRS panchromatic image prove to be essential in developing detailed and accurate road-access maps and effectively planning fieldwork. The major obstacles to surficial mapping in northern Alberta are boreal forest cover and very limited ground access. Processed, high-resolution, natural-colour images derived from Landsat and IRS play a crucial role for surficial mapping by providing information on recently created road access and land cover. Information on topographic and geomorphological features, regional glaciation and ice-flow pattern (*see* [Figure 4](#)), and land-cover types can also be obtained from remotely sensed data prior to fieldwork. This information helps to effectively plan field observation sites and carry out the surficial mapping process.

Surficial geological features, such as wetlands, flutings, meltwater channels, stagnant ice hummocks, sand dunes, alluvial fans and meandering rivers, can be recognized from processed remote-sensing data, and the boundaries of some of these features can be determined. Remote-sensing data, however, were unable to define the boundaries of the major map units, including moraine, glaciolacustrine deposits and bedrock. Ground-truthing and the experience of surficial geologists are crucial to interpretation. Satellite images also prove to be important for mapping regional and late-stage ice-flow directions in northern Alberta (Fenton et al., 2003b; Paulen and McClenaghan, in press). In addition, remote sensing can provide geologists with an overview of general land-cover type and morphology, which assists in understanding the surficial geological history.

Although satellite images can be used for producing maps of surficial-material potential at a moderate resolution (*see* [Figure 29](#)), remote sensing using satellite images has limitations for more detailed surficial mapping compared to aerial photographs. Overlapping stereo airphotos have a much higher image resolution and can be viewed in three dimensions with a stereoscope. The stereoscopic effect is crucial for precisely delineating boundaries of surficial material. Although shaded-relief effect can be incorporated in processed satellite images (e.g., *see* [Figures 23–25, 28](#)), the resolution is inadequate for precise delineation of surficial material boundaries, except for some wetland and sand dune boundaries. This study shows that satellite images can be used effectively in supporting the surficial mapping program currently undertaken by the AGS. It cannot, however, replace the existing airphoto approach in 1:100 000-scale surficial mapping.

Remote sensing also revealed a complex ice-flow pattern for the study area, with ice flowing southwest in the Fort Nelson Lowland and in the Fort Vermilion lowland ([Figure 4](#)). The surficial material in NTS area 84K ([Figure 29](#)) is represented by till in the uplands, which was laid down by the Late Wisconsinan glaciation. Afterwards, glaciolacustrine deposits blanketed the till in the lowlands. Then, eolian sand deposits developed above the glaciolacustrine plain after the drainage of glacial Lake Peace. Wetland and fluvial processes continue to shape and develop the present-day landscape.

7 References

- Alberta Energy (2002): Alberta Mineral Development Strategy; Alberta Energy, URL <http://www.energy.gov.ab.ca/docs/minerals/pdfs/Mineral_Strategy.pdf>, 24 p. {Sep 2005}.
- Barnett, P.J., Singhroy, V.H., Shirota, J. and Leney, S.J. (2004): Methods for remote engineering geology terrain analysis in boreal forest regions of Ontario, Canada; *Environmental and Engineering Geoscience*, v. 10, p. 229–241.
- Bayrock, L.A. (1961): Surficial geology; *in* Exploratory Soil Survey of Alberta Map Sheets 84M, 84N and 84O, J.D. Lindsay, S. Pawluk and W. Odynsky (ed.), Alberta Research Council, Preliminary Soil Survey Report 61-1, 43 p.
- Bélanger, J.R. (1980): Studies in Quaternary geology: an approach using remote sensing information; *in* Current Research, Part B, Geological Survey of Canada, Paper 80-1B, p. 287.
- Bélanger, J.R. (1983): Surficial geology mapping using remote sensing; *in* Current Research, Part A, Geological Survey of Canada, Paper 83-1A, p. 465–468.
- Bélanger, J.R. (1988): La cartographie des formations géologiques en surface a l'aide de la télédétection; Geological Survey of Canada, Paper 87-20, 21 p.
- Blais, A., Stevens, W.R., Graham, D.F. and Singhroy, V.H. (1995): A preliminary assessment of remote sensing as a tool for mapping surficial sediments in the southern Canadian Prairies; *in* Current Research 1995-B, Geological Survey of Canada, p. 141–149.
- Bobrowsky, P.T. and Rutter, N.W. (1992): The Quaternary geologic history of the Canadian Rocky Mountains; *Géographie physique et Quaternaire*, v. 46, p. 5–50.
- Bostock, H.S. (1970): Physiographic regions of Canada; Geological Survey of Canada, Map 1254A, scale 1:5 000 000.
- Boulton, G.S. and Clark, C.D. (1990): A highly mobile Laurentide Ice Sheet revealed by satellite images of glacial lineations; *Nature*, v. 346, p. 813–817.
- Brown, O., Utting, D., Little, E., Grunsky, E. and Harris, J. (2005): Remote predictive and enhanced surface-features mapping using analysis techniques on RADARSAT-1 and LANDSAT™ data on northern Baffin Island, Nunavut, Canada; *in* 35th Annual International Arctic Workshop, March 9–12, 2005, University of Alberta, Edmonton, Alberta, abstract on CDROM.
- Burns, J.A. (1996): Vertebrate paleontology and the alleged ice-free corridor: the meat of the matter; *Quaternary International*, v. 32, p. 107–112.
- Dreimanis, A. (1988): Tills, their genetic terminology and classification; *in* Genetic Classification of Glaciogenic Deposits, R.P. Goldthwait and C.L. Matsch (ed.), A.A. Balkema, Rotterdam, p. 17–67.
- Dyke, A.S. (2004): An outline of North American deglaciation with emphasis on central and northern Canada; *in* Quaternary Glaciations — Extent and Chronology, Part II: North America, J. Ehlers and P.L. Gibbard (ed.), Elsevier, Developments in Quaternary Science, p. 373–424.
- Dyke, A.S., Moore, A. and Robertson, L. (2003): Deglaciation of North America; Geological Survey of Canada, Open File 1574, 32 maps, scale 1:30 000 000.
- Eccles, D.R., Grunsky, E.C., Grobe, M. and Weiss, J. (2001): Structural emplacement model for kimberlitic diatremes in northern Alberta; Alberta Energy and Utilities Board, EUB/AGS Earth Sciences Report 2000-01, 103 p.
- Edwards, W.A.D and Scafe, D. (1996): Mapping and resource evaluation of the Tertiary and preglacial

- sand and gravel formations of Alberta; Alberta Research Council, AGS Geological Survey, Open File Report 1994-06, 241 p.
- Fenton, M.M. (1984): Quaternary stratigraphy, Canadian Prairies; *in* Quaternary Stratigraphy of Canada — A Canadian Contribution to IGCP Project 24, R.J. Fulton (ed.), Geological Survey of Canada, Paper 84-10, p. 57–68.
- Fenton, M.M. and Weiss, J.A. (2003): Preliminary report on contribution of satellite data to surficial mapping; north Buffalo Head Hills (NTS areas 84B/NW, 84C/NE, 84G, 84F/W); *in* 12th Annual Calgary Mining Forum and Alberta Geological Survey Minerals Section Open House, “Meeting Future Challenges in the Mineral Industry” 2003, Calgary, Program with Abstracts, p. 65.
- Fenton, M.M., Paulen, R.C. and Pawlowicz, J.G. (2003a): Evidence of pre-Late Wisconsin glacial deposits in central and northern Alberta; Canadian Quaternary Association (CANQUA), Annual Meeting, Halifax, Nova Scotia, Program and Abstracts, p. A28.
- Fenton, M.M., Pawlowicz, J.G., Paulen, R.C., Prior, G.J. and Olson, R.A. (2003b): Quaternary geology of northern Alberta: implications for kimberlite exploration; *in* VIII International Kimberlite Conference, Victoria, British Columbia, Conference Program and Extended Abstracts, 5 p.
- Fox J.C., Richardson R.J.H., Gowan R. and Sham P.C. (1987): Surficial geology of the Peace River – High Level area, Alberta; Alberta Research Council, Map 205, scale 1:500 000.
- Graham, D.F. and Grant, D.R. (1994): Airborne SAR for surficial geologic mapping; Canadian Journal of Remote Sensing, v. 20, no. 3, p. 319–323.
- Green, R., Mellon, G.B. and Carrigy, M.A. (1970): Bedrock geology of northern Alberta, NTS 84 and NTS 74D, 74E, 74L and 74M; Alberta Research Council, Alberta Geological Survey, Map 24, scale 1:500 000.
- Grunsky, E.C. (2002a): Satellite imagery catalogue; Alberta Energy and Utilities Board, EUB/AGS Geo-Note 2002-18, 24 p.
- Grunsky, E.C. (2002b): The application of principal components analysis to multi-beam RADARSAT-1 satellite imagery — a tool for land cover and terrain mapping; Canadian Journal of Remote Sensing, v. 28, no. 6, p. 758–769.
- Gupta, R.P. (1991): Remote Sensing Geology; Springer-Verlag, New York, 356 p.
- Halsey, L.A., Vitt, D.H. and Bauer, I.E. (1998): Peatland initiation during the Holocene in continental western Canada; Climatic Change, v. 40, p. 315–342.
- Hamilton, W.N., Price, M.C. and Langenberg, C.W. (1999): Geological map of Alberta; Alberta Energy and Utilities Board, EUB/AGS Map 236, scale 1:1 000 000.
- Harris, J.R., Bowie, C., Rencz, A.N. and Graham, D. (1994): Computer enhancement techniques for the integration of remotely sensed, geophysical, and thematic data for the geosciences; Canadian Journal of Remote Sensing, v. 20, no. 3, p. 210–221.
- Harris, J.R., Eddy, B., Rencz, A., de Kemp, E., Budkewitsch, P. and Peshko, M. (2001): Remote sensing as a geological mapping tool in the Arctic: preliminary results for Baffin Island, Nunavut; Geological Survey of Canada, Current Research, 2001-E12, 20 p.
- Henderson, E.P. (1959): Surficial geology of Sturgeon Lake map-area, Alberta; Geological Survey of Canada, Memoir 303, 108 p.
- Kettles, I.M., Rencz, A. and Bauke, S.D. (1998): Integration of Landsat and geological data as an aid to mapping glacial sediments in the Manitouwadge area, Ontario; Geological Society of America, Abstracts with Program, v. 30, p. 358.

- Lemmen, D.S., Duk-Rodkin, A. and Bednarski, J. (1994): Late glacial drainage systems along the northwestern margin of the Laurentide ice sheet; *Quaternary Science Reviews*, v. 13, p. 805–828.
- Levson, V.M. and Ferbey, T. (2004): Pleistocene stratigraphy of the Boreal Plains in northeasternmost British Columbia; *in* Geological Association of Canada–Mineralogical Association of Canada Joint Annual Meeting, St. Catherines, Ontario, May 2004, Program and Abstracts, v. 29, p. 35.
- Levson, V.M., Ferbey, T., Kerr, B., Johnsen, T., Bednarski, J., Smith, I.R., Blackwell, J. and Jonnes, S. (2004): Quaternary geology and aggregate mapping in northeast British Columbia: application for oil and gas exploration and development; *in* Summary of Activities, British Columbia Ministry of Energy and Mines, Resource Development and Geoscience Branch, p. 29–40.
- Lindsay, J.D., Pawluk, S. and Odynsky, W. (1960): Exploratory soil survey of Alberta map sheets 84J, 84K and 84L; Research Council of Alberta, Preliminary Soil Survey Report 60-1.
- Lowman, P.D., Harris, J., Masuoka, P.M., Singhroy, V.H. and Slaney, V.R. (1987): Shuttle imaging Radar (SIR-B) investigations of the Canadian Shield: initial report; *IEEE Transactions on Geoscience and Remote Sensing*, v. GE-25, no. 1, p. 55–66.
- Luscombe, A.P., Ferguson, I., Shepherd, N., Zimcik, D.G. and Naraine, P. (1993): The RADARSAT synthetic aperture radar development; *Canadian Journal of Remote Sensing*, v. 19, no. 4, p. 298–310.
- Masuoka, P.M., Harris, J., Lowman, P.D. and Blodget, H.W. (1988): Digital processing of orbital radar data to enhance geologic structure: examples from the Canadian Shield; *Photogrammetric Engineering and Remote Sensing*, v. 54, no. 5, p. 621–632.
- Mathews, W.H. (1980): Retreat of the last ice sheets in northeastern British Columbia and adjacent Alberta; *Geological Survey of Canada, Bulletin* 331, 22 p.
- Mei, S. (2004a): Orthorectified and principal component RADARSAT-1 image dataset for NTS 84K, Alberta; Alberta Energy and Utilities Board, EUB/AGS Geo-Note 2003-30, 10 p.
- Mei, S. (2004b): Orthorectified and principal component RADARSAT-1 image dataset for NTS 84L, Alberta; Alberta Energy and Utilities Board, EUB/AGS Geo-Note 2003-31, 10 p.
- Mei, S., Pana, D., Fenton, M. and Olson, R. (2005): Preliminary surficial lineaments mapping for the Maybelle River area, northeast Alberta, using remote sensing data; Alberta Energy and Utilities Board, EUB/AGS Earth Sciences Report 2004-02, 62 p.
- Mollard, J.D. (1996): Landforms and surface materials of Canada: a stereoscopic airphoto atlas and glossary (8th edition); PrintWest, Regina, Saskatchewan, 415 p.
- Moon, W.M., Won, J.S., Singhroy, V. and Lowman, P.D. (1994): ERS-1 and CCRS C-SAR data integration for look-direction bias correction using wavelet transform; *Canadian Journal of Remote Sensing*, v. 20, no. 3, p. 280–285.
- Paganelli, F. and Rivard, B. (2002): Contribution of the synergy of RADARSAT-1 and seismic imagery interpretation in the structural geology of the Central Alberta Foothills, Canada, as an aid for oil and gas exploration; *Canadian Journal of Remote Sensing*, v. 28, no. 5, p. 686–700.
- Paganelli, F., Grunsky, E.C. and Richards, J.P. (2001): Structural interpretation of RADARSAT-1 principal component imagery and its potential application to kimberlite exploration in the Buffalo Head Hills area, northern central Alberta; Alberta Energy and Utilities Board, EUB/AGS Special Report 21, 52 p.
- Paganelli, F., Grunsky, E.C., Richards J.P. and Pryde R. (2003): Use of RADARSAT-1 principal component imagery for structural mapping: a case study in the Buffalo Head Hills area, northern central Alberta, Canada; *Canadian Journal of Remote Sensing*, v. 29, no. 1, p. 111–140.

- Paulen, R.C. (2004): Surficial geology of the Grimshaw area (NTS 84C/SW); Alberta Energy and Utilities Board, EUB/AGS Map 291, scale 1:100 000.
- Paulen, R.C. and McClenaghan, M.B. (in press): Late Wisconsin ice flow history in the Buffalo Head Hills kimberlite field; *in* Current Research, Geological Survey of Canada.
- Paulen, R.C., Fenton, M.M. and Bobrowsky, P.T. (2003): Spectacular, large-scale deformation structures in glaciolacustrine sediments, Peace River, Alberta, Canada; *in* 16th INQUA Congress, Reno, Nevada, July 23–30, 2003, Program with Abstracts, p. 64.
- Paulen, R.C., Fenton, M.M., Pawlowicz, J.G., Smith, I.R. and Plouffe, A. (2005a): Surficial geology of the Little Hay River (NTS 84L/NW); Alberta Energy and Utilities Board, EUB/AGS Map 315, scale 1:100 000.
- Paulen, R.C., Fenton, M.M., Weiss, J.A., Pawlowicz, J.G., Plouffe, A. and Smith, I.R. (2005b): Surficial geology of the Hay Lake area (NTS 84L/NE); Alberta Energy and Utilities Board, EUB/AGS Map 316, scale 1:100 000.
- Paulen, R.C., Plouffe, A., Smith, I.R., Fenton, M.M., Pawlowicz, J.G., Weiss, J.A., Kowalchuk, C.J. and Trommelen, M.S. (2004): Surficial geology of the Zama Lake area (NTS 84L); *in* Geological Association of Canada–Mineralogical Association of Canada, Joint Annual Meeting, St. Catherines, Ontario, May 2004, Program with Abstracts, v. 29, p. 458.
- Pettapiece, W.W. (1986): Physiographic subdivisions of Alberta; Agriculture Canada, Research Branch, Land Resource Research Centre, physiographic map, scale 1:1 500 000.
- Plouffe, A., Smith, I.R., Paulen, R., Fenton, M. and Pawlowicz, J.G. (2004): Surficial geology, Bassett Lake, Alberta (NTS 84L SE); Geological Survey of Canada, Open File 4637, surficial map, scale 1:100 000.
- RADARSAT International (RSI) (1999): RADARSAT illuminated: your guide to products and services; RADARSAT International, RADARSAT user guide, 113 p.
- British Columbia Resources Inventory Committee (1996): Guidelines and standards to terrain mapping in British Columbia; British Columbia Ministry of Sustainable Resource Management, Resources Inventory Committee, Publication 12, 216 p.
- Richards, J.A. (1986): Remote Sensing Digital Image Analysis; Springer-Verlag, New York, 281 p.
- Sabins, F. (1992): Remote Sensing: Principles and Interpretation (2nd edition); W.H. Freeman and Co., New York, 449 p.
- Sauer, E.K. and Elder, L. (1982): Airphoto interpretation for terrain analysis: a guidebook to J.D. Mollard's *Landforms and Surface Materials of Canada*; University of Saskatchewan Press, Saskatoon, Saskatchewan, 240 p.
- Singhroy, V. and Saint-Jean, R. (1999): Effects of relief on the selection of RADARSAT-1 incidence angle for geological applications; *Canadian Journal of Remote Sensing*, v. 25, no. 3, p. 211–217.
- Singhroy, V., Slaney, R., Lowman, P., Harris, J. and Moon, W. (1993): RADARSAT and radar geology in Canada; *Canadian Journal of Remote Sensing*, v. 19, no. 4, p.338–351.
- Smith, I.R., Plouffe, A., Paulen, R.C., Fenton, M. and Pawlowicz, J.G. (2005): Surficial geology, Hay River, Alberta (NTS 84L SW); Geological Survey of Canada, Open File 4754, surficial map, scale 1:100 000.
- Smith, I.R., Paulen, R.C., Plouffe, A., Kowalchuk, C. and Peterson, R. (2005): Surficial mapping and granular aggregate resource assessment in Northwest Alberta; *in* Summary of Activities 2005, BC Ministry of Energy and Mines, p. 80–95.

Smith S.K., Grieve, R.A.F., Harris, J.R. and Singhroy, V. (1999): The utilization of RADARSAT-1 imagery for the characterization of terrestrial impact landforms; *Canadian Journal of Remote Sensing*, v. 25, no. 3, p. 218–228.

Wolfe, S.A. (2002): Eolian deposits of the Prairie provinces of Canada; Geological Survey of Canada, Open File 4118, CD-ROM.

Appendix A — Ground-Truthing Sites in Map Area NTS 84K

Site ID	UTM11 Easting	UTM11 Northing	Unit	Vegetation	Geomorphology	Lithology	Genesis	Comments
JP04-47	502417	6473099	1	pasture	undulating veneer	fine sand	glaciolacustrine littoral	uncertain if recent fluvial or glaciolacustrine littoral; near intersection of two creeks
JP04-47	502417	6473099	2	pasture	undulating	clay	glaciolacustrine	mottled with brown, minor pink clay blebs, sharp contact with overlying sand
JP04-46	478304	6508733	1	forest-mixed	undulating	shale	bedrock	broken ironstone concretions on surface, platy, thin stony lag
JP04-45	472612	6501738	1	forest-conifer	undulating	sand	bedrock	shale with minor mudstone; strongly oxidized; no glacial lag on surface
MF04-52	488448	6503075	1	forest-deciduous	undulating	diamicton	till	1.5 m in thickness; possible flute
MF04-51	476790	6504534	1	cutblock	ridge(s)	diamicton	till	A few clasts, 1.5 m in average thickness
MF04-51	476790	6504534	2	cutblock	ridge(s)	siltstone	bedrock	No gypsum, no iron stain, sharp contact with unit overlying till
MF04-50	471187	6500994	1	forest-mixed	ridge(s)	siltstone	bedrock	few very fine grained sandstone lenses; sample collected for palynology
MF04-49	548786	6494614	1	pasture	plain	diamicton	till	boulders on the Fort Vermilion Grazing Ranch
MF04-48	531757	6473356	1	forest-deciduous	ridge(s)	sand	eolian	plain with ridges; very fine sand, well sorted, clast free, 3 m in thickness
MF04-48	531757	6473356	2	forest-deciduous	ridge(s)	silty clay	glaciolacustrine	sharp contact with the overlying very fine sand
MF04-47	513715	6495187	1	forest-mixed	plain	diamicton	glaciolacustrine	waterlain diamicton, abundant clasts
MF04-46	513707	6498748	1	forest-mixed	plain	silty clay	glaciolacustrine	abundant dropstones
MF04-45	513563	6499564	1	forest-deciduous	plain	clayey silt	uncertain	1 m in thickness, wet, no clasts
MF04-45	513563	6499564	2	forest-deciduous	plain	clayey silt	glaciolacustrine	contact with unit 1 is where cut into a firmer silty clay layer, about 2 cm thick; below this back into clayey silt; both units are similar, both units organic free; possible alluvium over glaciolacustrine, or glaciolacustrine
JP04-44	547787	6492770	1	pasture	plain	diamicton	till	faint bedding, possibly water-laid diamicton
JP04-43	513710	6497701	1	forest-deciduous	undulating	silty clay	glaciolacustrine	glaciolacustrine clay, minor stony lag on surface; possibly ice-rafted debris or dropstones

Site ID	X	Y	Unit #	Vegetation	Geomorphology	Lithology	Genesis	Comments
JP04-42	513699	6499183	1	forest-mixed	undulating	silty clay	glaciolacustrine	laminated
JP04-42	513699	6499183	2	forest-mixed	undulating	sand	glaciolacustrine	Littoral glaciolacustrine sand?
JP04-42	513699	6499183	3	forest-mixed	undulating	silty clay	glaciolacustrine	pink clay bed
MF04-41	476394	6447131	1	forest-deciduous	plain	silty clay	glaciolacustrine	dark grey clay laminae; sharp lower contact; dropstones.
MF04-41	476394	6447131	2	forest-deciduous	plain	diamicton	till	A well-developed boulder pavement within till; pavement top striations are 252°.
MF04-40	469328	6431122	1	forest-deciduous	plain	silty clay	glaciolacustrine	very calcareous firm moist glaciolacustrine clay
MF04-39	458024	6441668	1	forest-mixed	plain	diamicton	glaciolacustrine	Layered waterlain diamicton with some discontinuous silt layers; very calcareous; sharp lower contact with unit 2.
MF04-39	458024	6441668	2	forest-mixed	plain	diamicton	till	Massive; very calcareous; contact looks like interaction between proglacial lake and ice margin.
JP04-39	480426	6456503	1	forest-deciduous	undulating	silt	glaciolacustrine	massive
JP04-39	480426	6456503	2	forest-deciduous	undulating	silty clay	glaciolacustrine	Silt in lower 10 cm, upper 30 cm silty clay, fining upwards
JP04-38	479786	6456314	1	wetland	plain	peat	organic	
JP04-37	481289	6447237	1	forest-deciduous	plain	clayey silt	glaciolacustrine	Mostly massive with laminations in lower 0.5 m
JP04-36	479133	6447185	1	forest-deciduous	plain	silty clay	glaciolacustrine	massive, brown, oxidized
JP04-35	462584	6437693	1	forest-mixed	plain	silt	glaciolacustrine	Sandy silt, 0.5 m in thickness, no Lamination
JP04-35	462584	6437693	2	forest-mixed	plain	silty clay	glaciolacustrine	massive, with dropstones
JP04-41	550434	6437987	1	forest-deciduous	plain	silt	glaciolacustrine	site located in trees on a lobe of a possible fan
JP04-41	550434	6437987	2	forest-deciduous	plain	silty clay	glaciolacustrine	massive
JP04-40	532030	6443854	1	forest-mixed	hummock(s)	sand	eolian	sand pit
MF04-44	538448	6457532	1	cultivated	ridge(s)	sand	Glaciolacustrine littoral	Ridges about 2 m in relief form a "finger print" pattern on the Satellite images; Also possibly eolian
MF04-44	538448	6457532	2	cultivated	ridge(s)	clayey silt	glaciolacustrine	rhythmically bedded silt and clay
MF04-43	550715	6438026	1	wetland	plain	peat	organic	Dry bog on fen

Site ID	X	Y	Unit #	Vegetation	Geomorphology	Lithology	Genesis	Comments
MF04-43	550715	6438026	2	wetland	plain	clayey silt	Glaciolacustrine littoral	laminated silt and clay, sharp lower contact; origin may be shallow water lake on sediments washed down from Buffalo Head Hills to the south
MF04-43	550715	6438026	3	wetland	plain	clayey silt	glaciolacustrine	Firm, slightly mottled, laminated silt and clay, one band at 2.3 m may be organic clay or coal
MF04-42	505812	6431703	1	cultivated	hummock(s)	silty clay	glaciolacustrine	Hummocks about 2m high; pattern in surrounding flat region may also be result of low relief hummocks.

X and Y co-ordinates are based on NAD83 datum and UTM11 map projection.